UNITED STATES
PARTMENT OF
OMMERCE
UBLICATION

NBS TECHNICAL NOTE 609

Study of Cryogenic Storage Tank Fatigue Life

Low Temperature Mechanical Testing of AISI 304 and 310 Stainless Steels

U. S.
PARTMENT
OF
OMMERCE
National
Bureau
of
Standards

NATIONAL BUREAU OF STANDARDS

The National Bureau of Standards[1] was established by an act of Congress March 3, 1901. The Bureau's overall goal is to strengthen and advance the Nation's science and technology and facilitate their effective application for public benefit. To this end, the Bureau conducts research and provides: (1) a basis for the Nation's physical measurement system, (2) scientific and technological services for industry and government, (3) a technical basis for equity in trade, and (4) technical services to promote public safety. The Bureau consists of the Institute for Basic Standards, the Institute for Materials Research, the Institute for Applied Technology, the Center for Computer Sciences and Technology, and the Office for Information Programs.

THE INSTITUTE FOR BASIC STANDARDS provides the central basis within the United States of a complete and consistent system of physical measurement; coordinates that system with measurement systems of other nations; and furnishes essential services leading to accurate and uniform physical measurements throughout the Nation's scientific community, industry, and commerce. The Institute consists of a Center for Radiation Research, an Office of Measurement Services and the following divisions:

> Applied Mathematics—Electricity—Heat—Mechanics—Optical Physics—Linac Radiation[2]—Nuclear Radiation[2]—Applied Radiation[2]—Quantum Electronics[3]—Electromagnetics[3]—Time and Frequency[3]—Laboratory Astrophysics[3]—Cryogenics[3].

THE INSTITUTE FOR MATERIALS RESEARCH conducts materials research leading to improved methods of measurement, standards, and data on the properties of well-characterized materials needed by industry, commerce, educational institutions, and Government; provides advisory and research services to other Government agencies; and develops, produces, and distributes standard reference materials. The Institute consists of the Office of Standard Reference Materials and the following divisions:

> Analytical Chemistry—Polymers—Metallurgy—Inorganic Materials—Reactor Radiation—Physical Chemistry.

THE INSTITUTE FOR APPLIED TECHNOLOGY provides technical services to promote the use of available technology and to facilitate technological innovation in industry and Government; cooperates with public and private organizations leading to the development of technological standards (including mandatory safety standards), codes and methods of test; and provides technical advice and services to Government agencies upon request. The Institute also monitors NBS engineering standards activities and provides liaison between NBS and national and international engineering standards bodies. The Institute consists of the following technical divisions and offices:

> Engineering Standards Services—Weights and Measures—Flammable Fabrics—Invention and Innovation—Vehicle Systems Research—Product Evaluation Technology—Building Research—Electronic Technology—Technical Analysis—Measurement Engineering.

THE CENTER FOR COMPUTER SCIENCES AND TECHNOLOGY conducts research and provides technical services designed to aid Government agencies in improving cost effectiveness in the conduct of their programs through the selection, acquisition, and effective utilization of automatic data processing equipment; and serves as the principal focus within the executive branch for the development of Federal standards for automatic data processing equipment, techniques, and computer languages. The Center consists of the following offices and divisions:

> Information Processing Standards—Computer Information—Computer Services—Systems Development—Information Processing Technology.

THE OFFICE FOR INFORMATION PROGRAMS promotes optimum dissemination and accessibility of scientific information generated within NBS and other agencies of the Federal Government; promotes the development of the National Standard Reference Data System and a system of information analysis centers dealing with the broader aspects of the National Measurement System; provides appropriate services to ensure that the NBS staff has optimum accessibility to the scientific information of the world, and directs the public information activities of the Bureau. The Office consists of the following organizational units:

> Office of Standard Reference Data—Office of Technical Information and Publications—Library—Office of Public Information—Office of International Relations.

---

[1] Headquarters and Laboratories at Gaithersburg, Maryland, unless otherwise noted; mailing address Washington, D.C. 20234.
[2] Part of the Center for Radiation Research.
[3] Located at Boulder, Colorado 80302.

UNITED STATES DEPARTMENT OF COMMERCE
Maurice H. Stans, Secretary
U.S. NATIONAL BUREAU OF STANDARDS • Lewis M. Branscomb, Director

NBS TECHNICAL NOTE 609

ISSUED AUGUST 1971

Nat. Bur. Stand. (U.S.), Tech. Note 609, 86 pages (Aug. 1971)
CODEN: NBTNA

Study of Cryogenic Storage Tank Fatigue Life

Low Temperature Mechanical Testing of AISI 304 and 310 Stainless Steels

R. P. Reed, R. L. Durcholz, R. E. Schramm, and T. J. Patrician

Cryogenics Division
Institute for Basic Standards
National Bureau of Standards
Boulder, Colorado 80302

Sponsored by
Naval Air Engineering Center
Philadelphia, Pennsylvania
under Project Order 9-8029

NBS Technical Notes are designed to supplement the Bureau's regular publications program. They provide a means for making available scientific data that are of transient or limited interest. Technical Notes may be listed or referred to in the open literature.

For sale by the Superintendent of Documents, U.S. Government Printing Office, Washington, D.C. 20402
(Order by SD Catalog No. C13.46:609), Price 75 cents

Contents

List of Tables

List of Figures

Page

Page

STUDY OF CRYOGENIC STORAGE TANK FATIGUE LIFE

Low Temperature Mechanical Testing of AISI 304 and 310 Stainless Steels

R. P. Reed, R. L. Durcholz, R. E. Schramm, and T. J. Patrician

Two 300 series stainless steels were tested for impact-fatigue life and tensile properties as a function of temperature, percent transformed phase (martensite), stress level, and specimen geometry. These alloys were studied to predict the fracture characteristics of parent material and weld joints in large cryogenic dewars which are subjected to periodic stresses. Normally, AISI 304 is employed in the construction of such dewars. Under fatigue loading conditions at cryogenic temperatures, the behavior of AISI 304 is complicated by the gradual transformation to a martensitic structure. The influence of this transformation on the fracture characteristics was studied. For this purpose, a new impact-fatigue test and necessary equipment were developed.

The fatigue strength of AISI 304 and 310 exhibit similar trends, but at a given fatigue life and temperature, the fatigue strength of AISI 304 is slightly superior. AISI 310 displays an endurance limit of about 20,000 psi;* the 304 limit is 25-30,000 psi. However, the lowest endurance limit (weakest) specimens appear to be the triaxially-loaded AISI 304 weld specimens which have an endurance limit near 10,000 psi. Little temperature-dependence of the impact-fatigue properties was observed.

Key words: Fatigue; fracture; impact; low temperature; mechanical property equipment; stainless steel.

---

* For ease in interpretation all stress values in the text are expressed in units of psi. Conversion to other stress units are 10^3 psi = 0.703 kg/mm^2 = 6.90×10^6 N/m^2.

1. Summary

The principal results of this report are briefly summarized below.

1. The impact-fatigue strength of AISI 304 is superior or equal to the impact-fatigue strength of AISI 310 under all conditions in the temperature range 76 to 294K.
2. The endurance limit generally appears at about 10^5 cycles. At all temperatures (294, 195, 76K), the limit can be roughly approximated by using the room temperature tensile yield strength. Possible critical exceptions are under triaxial stresses at 195 and 76K, where the endurance limit is less than the room temperature yield stress. In these cases, a considerable extra safety factor in designing is desired.
3. Welds exhibit less strength under impact-loading conditions than the parent material: under uniaxial loading conditions, approximately a 10% reduction was found; under biaxial conditions about a 15% reduction was found. Although triaxial loading conditions could not be tested, on the basis of our results, it is expected that this configuration (weld, triaxially applied stress) at low temperature would prove the weakest link in any structure.
4. Cold working (11%) at 76K produces a 35-50% increase in AISI 310 fatigue strength and a 40-55% increase in AISI 304 fatigue strength.
5. The transformation to martensite during repeated impact cycles has little deleterious effect on fatigue life. Under uniaxial and biaxial loading conditions, the transformation

is beneficial, increasing the fatigue strength.

6. In the case of AISI 304, there is a good possibility of monitoring the fatigue life by measurement of the amount of ferromagnetic phase (martensite) by simple magnetic techniques.
7. Two studies remain in order to insure the mechanical stability at cryogenic temperatures of AISI 300 series stainless steels, undergoing partial martensitic transformations. These are: the impact-fatigue strength in the temperature range 4 to 76K and the influence on martensitic transformations and mechanical stability of differences in weld techniques.

2. Introduction

The objective of this study is to predict the life of AISI 300 series stainless steel parent material and weld joints when subjected to periodic large, sudden stresses in the temperature range 300 to 76K. At present, knowledge concerning the endurance life and effects of martensitic transformation on fatigue strength is not available. To enable safe transport of liquid oxygen in large quantities (400 gallons and up), such knowledge must be obtained, since most dewar systems are now fabricated with AISI 304 stainless steel. Actual conditions were simulated to provide the most useful information to dewar design.

Brittle failure, from analysis of accident investigations, is listed as a factor of primary importance in causing system failures in cryogenic equipment. The continual exposure of liquid oxygen tanks to high stresses (for example during the carrier on-deck delivery) poses a serious question of possible fatigue-transformation failure. Failure may occur for two reasons:

(1) When normal 304 stainless steel is stressed above its yield strength at temperatures below about 200K, a partial crystallographic transformation from austenite (face-centered cubic structure) to martensite (body-centered cubic structure) occurs. There is an associated local volume expansion of 4% caused by the transformation. This local volume expansion promotes very high stress concentrations in material that is not ductile, such as weld areas.

(2) Normal fatigue failure, under periodic stress above the yield stress, also may occur. The endurance or fatigue limit of the combination of 304 steel, weld joint, and large stresses has never been tested; and to our knowledge, no similar circumstances have been duplicated in previous usage. Therefore, prediction of tank and safety is very speculative.

Various types of fatigue tests have been devised and are identified in three general categories.

1. tension-compression
2. bending
3. torsion

The test specimen is subjected to constraints which fall into one of two classes,

1. constant load, bending moment, or torque.
2. constant strain, bending deflection, or twist.

To keep test times to a reasonable duration, the repetition frequency is usually on the order of 10^2 - 10^4 cycles/min. High frequencies can result in an artifically short life due to sample heating. There are, however, indications[1] that a low repetition rate, without any heating problem, can also lead to a short life.

Many investigations[2-13] have shown that the strain rate to which a metal is subjected does affect the microstructure and this, in turn, is reflected in the mechanical properties. A review of many of these influences has recently been published.[14] Of course, there are actual situations which are approximated poorly or not at all by the

[1] Superscripts indicate literature references listed at the end.

standard tests. Among these is the sudden impact loading or jolt delivered at a frequency of about one per hour or day, such as might happen during handling, transportation, or in the transfer of fluid through pipes.

To approximate better the actual environmental loading conditions, a new type of fatigue test was devised. This new test was performed on a commercial impact machine, modified to apply repeatedly the same impact load to the specimen (see Appendix). This report describes the tests carried out in the temperature range 76 to 297K, documents all test results, and discusses the significance of the data in terms of use in designing cryogenic equipment.

3. Test Materials, Specimen Preparation and Equipment

We tested two austenitic stainless steels, AISI 304 and 310; Table 1 gives the nominal composition of these alloys. AISI 310 is a crystallographically stable alloy with a face-centered cubic (fcc) structure, while annealed AISI 304 is known to undergo a martensitic phase transformation from fcc to hexagonal close-packed (hcp) and body-centered cubic (bcc) structures. This transformation always occurs on deformation of the 304 steel below room temperature, and, depending on the exact composition, may occur spontaneously on cooling to the vicinity of 76 K.[5]

Table 1.

Nominal Composition of AISI 304 and 310 Stainless Steels

AISI Type	Composition (%) C	Cr	Ni	Mn
304	0.08 max	18.0-20.0	8.00-11.00	2.00 max
310	0.25 max	24.0-26.0	19.0 -22.0	2.00 max

Specimens were tested in three configurations:

1. flat, smooth, (uniaxial).
2. flat, notched (biaxial).
3. round, notched (triaxial).

The notches cause the load to be broken down vectorially into longitudinal and transverse components. In this way the flat specimens are subjected to biaxial stresses while the round specimens see three-way or triaxial stresses. Dimensions are shown in Figure 1. The flat samples were cut from sheet parallel to the rolling direction, and the round specimens were produced from bar stock. By computing the stress concentration factor, K_t, from the formula

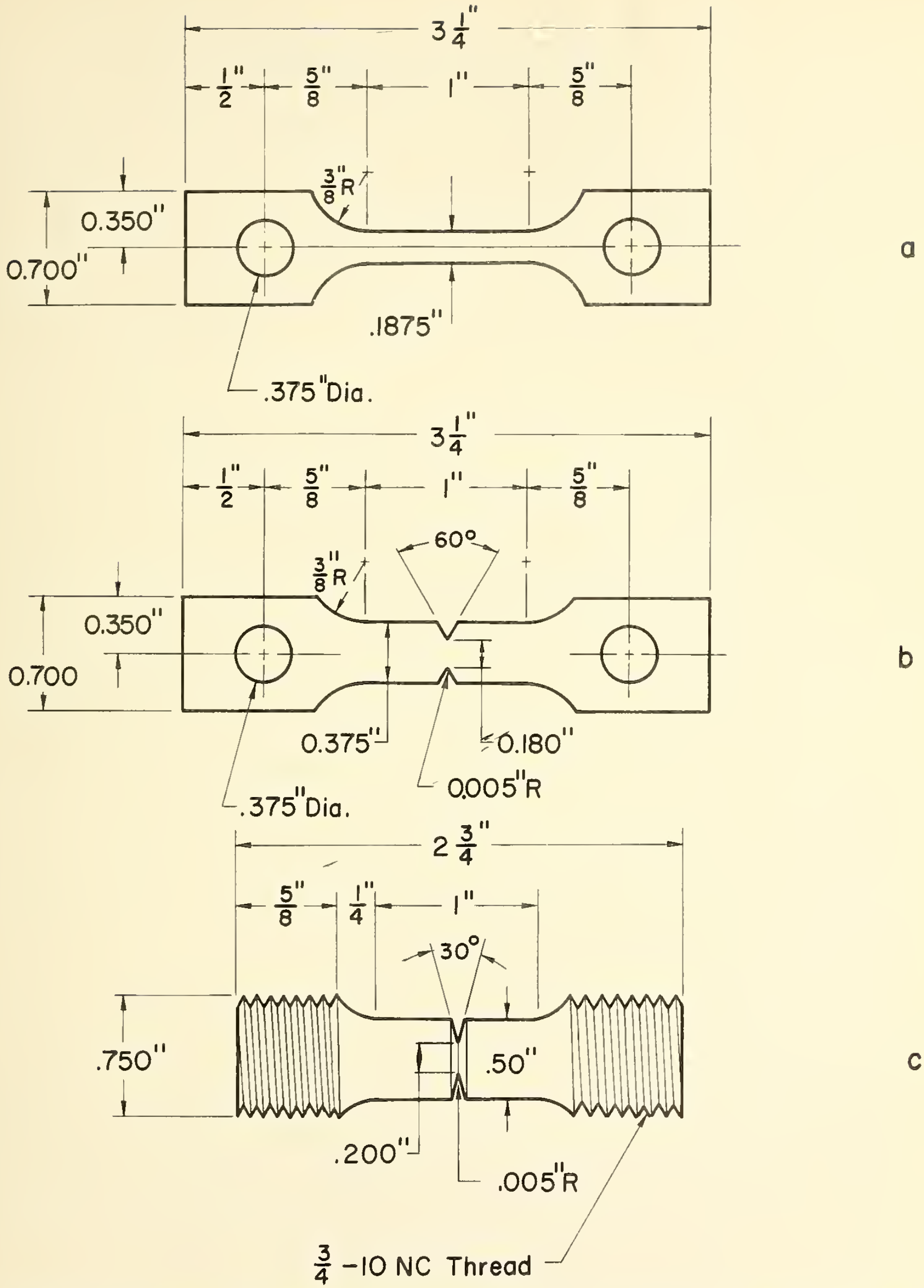

Figure 1. Sample geometries for tensile and impact tests: a. Uniaxial, thickness = 0.1 in; b. Biaxial, thickness = 0.1 in; c. Triaxial.

$$K_t = \sqrt{\frac{\frac{1}{2}\text{ distance between notches}}{\text{notch radius}}}$$

it has the value 4.2 and 4.5 for the biaxial and triaxial geometries, respectively. After machining, the flat samples were mechanically ground and polished. All samples were then vacuum annealed at 1000°C for one-half hour and air cooled. The majority of tests involved these materials as annealed, but some samples were subjected to further treatment to check the effect of chemical and physical variables on the impact fatigue life.

AISI 304 uniaxial and biaxial specimens, prepared from a melt which transformed spontaneously on cooling, were thermally cycled ten times between 297K and 76K. This produced about 2-7% martensitic products prior to the impact tests. Also, several 304 uniaxial specimens were held at 813K for three hours in air to test possible effects of sensitization, or the formation of intergranular carbides.

To get a quantitative idea of the influence of cold-work on impact-fatigue life, uniaxial specimens of both alloys were mounted on a tensile-testing machine and stressed at 76K to 11% strain; in the 304 this produced about 50% martensite. Those samples to be tested at 76K were maintained at that temperature until broken; the samples for the 297K tests were warmed just prior to use.

Welding introduces another very important variable. Welded plates were prepared from which uniaxial and biaxial samples were machined. Notches were ground both in the weld area and at two positions in the heat-affected zone. The technique was as follows:

material: AISI 304 stainless steel, 1/8 inch thick plate;
AISI 308 stainless steel weld rod, 0.035 inch diameter wire.

preparation: plates were machined, deburred, electrocleaned, rinsed, then electro polished. The caustic electrocleaning solution consisted of 8 oz. of Oakite* #160 per gallon. This was run at 160°F (344K) at 6 volts. The plates were electro polished in 70% phosphoric acid, 30% sulfuric acid at 140°F (333K) using 9 volts for 4 minutes. Finally, the plates were again rinsed in water.

welding procedure: weld was butt-type in a flat position, using machine welding techniques. One pass, using an average welding speed of 18 inches per minute, was made over a length of 20 inches. A 0.09 inch gap was maintained by tacking 3.5 inch intervals. The plates were held down pneumatically and a Pandjiris weld positioner was employed.

welding atmospheres: a mixture of 30% He and 70% Ar at an average flow of 10 cubic feet per hour was used.

inspection and finishing: weld beads were inspected using standard radiographic techniques for porosity. Welds of poor quality were rejected. Weld beads were then machined off, the sample was polished, and magnetic permeability measurements made using a Magne-Gage. No further heat treatment was used prior to testing.

The samples used in the microscopic analysis were of the uni-

---

*Trademark. Precise specification of the material employed has been necessary to make the description of this apparatus sufficiently meaningful. Identification of this material or its manufacturer by the National Bureau of Standards in no way implies a recommendation or endorsement by the Bureau. Furthermore, use of other trade names in this paper is for the sake of clarity and does not in any way imply a recommendation or endorsement by the Bureau.

axial geometry, but thinner and with a wider reduced section (Fig. 2). They were annealed as noted for the impact specimens.

The impact-fatigue tests were conducted using a Riehle impact machine which had undergone major modifications; the details on the automation of this device and the cryogenic system used with it are presented in a paper to be published in Section C, Journal of Research, NBS (See Appendix). A standard Instron testing machine served for the tensile tests. The amount of ferromagnetic bcc martensite produced during these tests was recorded by measurements with a Magne-Gage, an instrument consisting of standard bar magnets affixed to torsion balance equipment.

The microscopic studies were done with a standard optical metallograph and electron microscope.

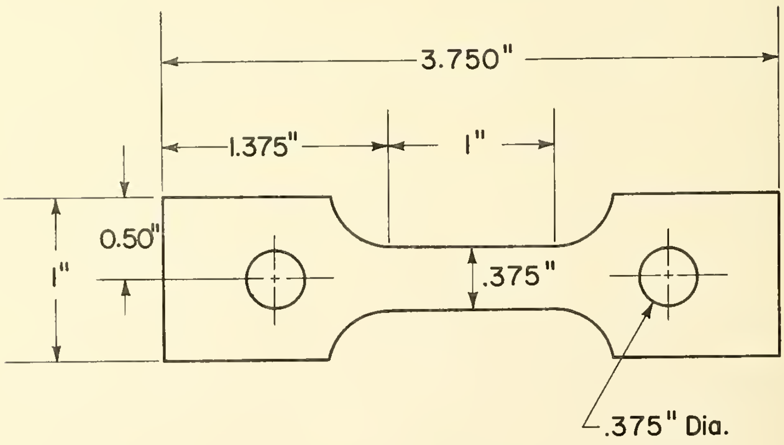

Figure 2. Electron microscopy specimen, thickness = 0.1 in.

4. Measurements and Calculations

In the documentation and description of our data, a number of symbols and definitions are employed. The following discussion identifies these.

Definitions of Symbols Used

A	Sample area outside necking region after fracture.
A_F	Sample area at fracture.
A_0	Initial sample area.
E	Elastic modulus.
E_F	Absorbed energy density required to deform sample.
e	Elongation in 1 inch.
L	Sample load.
ℓ	Gauge length just before necking.
ℓ_F	Gauge length after fracture.
ℓ_0	Initial gauge length.
N	Number of impact cycles to fracture.
RA	Reduction in area before necking.
RAN	Reduction in area at neck.
T	Temperature.
V	Sample volume after fracture.
V_0	Initial sample volume.
$\dot{\epsilon}$	Strain rate.
ϵ_E	Engineering strain.
ϵ_T	True strain.
σ_A	Applied or engineering stress.
σ_F	Fracture stress.
σ_T	True stress.
σ_u	Ultimate or tensile strength.
σ_y	Yield strength (.002 offset).

Direct measurements are made on:

A, A_F, A_0, L, ℓ_F, ℓ_0, N, T, and $\dot{\epsilon}$

During the tensile tests, a strip chart recorder was used to continuously note the engineering strain, ϵ_E, as a function of the sample load, L. The engineering stress, σ_A, is given by

$$\sigma_A = \frac{L}{A_0} .$$

The stress-strain curve was then easily constructed from the strip chart record and used to determine the ultimate and yield stresses, σ_u and σ_y, and the elastic modulus, E. Figure 3 illustrates this graphically.

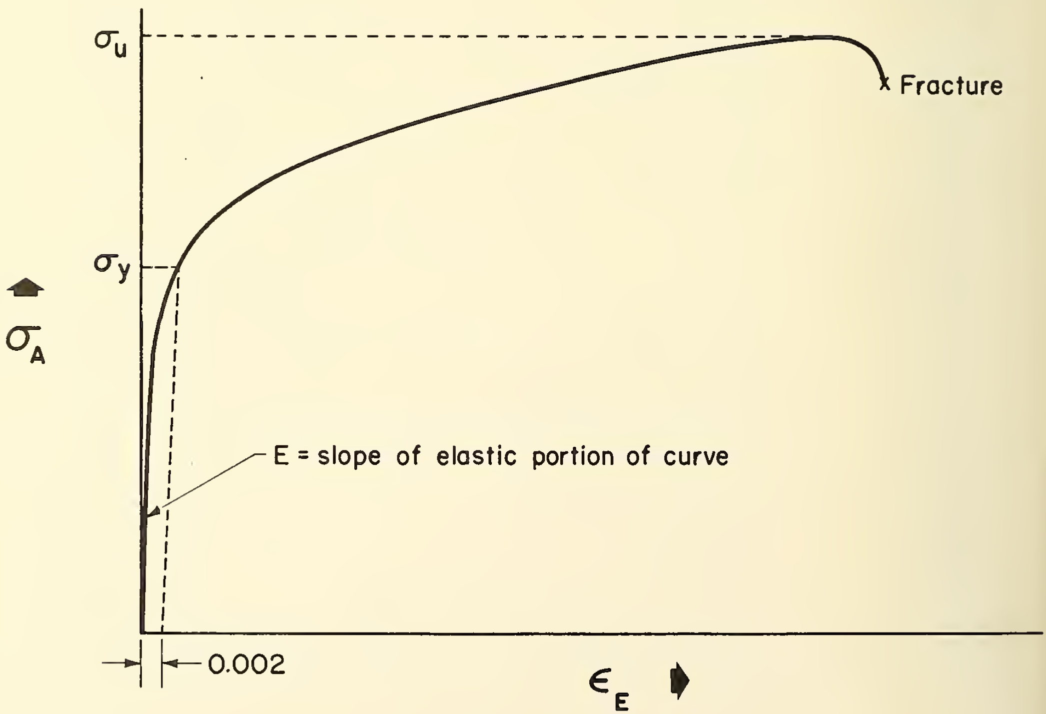

Figure 3. Determination of E, σ_u, and σ_y from a stress-strain curve.

Reductions of area and elongation are determined directly from sample measurements.

$$RA = \frac{A_0 - A}{A_0} = 1 - \frac{A}{A_0}$$

$$RAN = \frac{A_0 - A_F}{A_0} = 1 - \frac{A_F}{A_0}$$

$$e = \frac{\ell_F - \ell_0}{\ell_0}$$

In the notched samples, both biaxial and triaxial, little, if any, necking occurs so $A = A_F$ and $RA = RAN$.

Fracture stress is

$$\sigma_F = \frac{L}{A_F}$$

For the tensile tests this is most easily determined from

$$\sigma_F = \frac{\sigma_u}{1 - RAN}$$

While it is true that dislocations and vacancies are introduced into the crystalline structure during deformation, it is nearly true that the volume of the sample remains constant, i. e.

$$V = V_0 \quad .$$

So

$$\ell A = \ell_0 A_0 \quad ,$$

$$\frac{\ell}{\ell_0} = \frac{A_0}{A} \quad .$$

Since:

$$\epsilon_E = \frac{\ell - \ell_0}{\ell_0} = \frac{\ell}{\ell_0} - 1 \quad ,$$

it follows that

$$1 + \epsilon_E = \frac{1}{1 - RA} \quad ,$$

and

$$\epsilon_E = \frac{RA}{1 - RA} \quad .$$

From this the true strain can be determined.

$$\epsilon_T = \ell n \left(\frac{\ell}{\ell_0} \right) = \ell n \, (1 + \epsilon_E) \; .$$

The true stress is

$$\sigma_T = \frac{L}{A} \; .$$

Again assuming constant volume:

$$\sigma_T = \frac{L}{A_0} \; \frac{A_0}{A} = \sigma_A \; \frac{\ell}{\ell_0} = \sigma_A (1 + \epsilon_E) \; .$$

There are basically two stages in the fatigue life of a sample:

1. Uniform strain.
2. Necking followed by fracture.

Most of the energy is absorbed during the uniform strain portion. Once necking has begun, almost all further energy is concentrated in that small volume and fracture quickly follows. To make calculation possible, it is assumed that the only significant absorbed energy is that required to just bring the sample to the point of necking. The density of absorbed energy required to deform the sample is then:

$$E_F = \frac{L(\ell - \ell_0)}{V} = \frac{L(\ell - \ell_0)}{V_0} = \frac{L}{A_0} \; \frac{\ell - \ell_0}{\ell_0} \, ,$$

$$E_F = \sigma_A \, \epsilon_E \; .$$

5. Experimental Results

5.1 Mechanical--Impact

The impact-fatigue data for AISI 304 and 310 stainless steels are presented in Tables 2 and 3 and are plotted as S-N curves (applied stress vs. number of cycles) in Figures 4-11. The fatigue life curves in Figures 12-14 give a comparison of these two alloys for durations of 10^2, 10^3, and 10^4 cycles. Some results are immediately apparent from these curves:

(1) A decrease in temperature increases the impact-fatigue life.

(2) Fatigue life of uniaxially stressed specimens is generally longest, followed by biaxially stressed specimens. Specimens stressed under triaxial conditions are usually weakest.

(3) In the uniaxial configuration, the fatigue strength of 304 is superior to that of 310. At room temperature, the difference is about 5-15% and at 76K it is 25-30%. In Figures 7 and 8, the data for the 304 samples that were sensitized or precycled to 76K fall in line with the annealed points, indicating very little or no effect on the impact-fatigue behavior by these thermal treatments. This agrees with previous work on sensitized 304 subjected to high strain rates.[23]

(4) The shape of the curves in Figures 10 and 11 for the 304 weldments exhibit the same general behavior as the annealed material. In the uniaxial geometry, the strength is slightly reduced by welding; however, this decrease depends on temperature - about 20% at 297K and 8% at 76K for a life of 10^3 cycles. The results are similar for a 10^4 cycle life (Figure 14). The strength of biaxial samples is nearly unchanged at room temperature but reduced at 76K. The most remarkable thing here is the insensitivity of fatigue life to the relative position of weld and notch. In Figure 11, a single curve at each temperature could be drawn through the data points for all three notch positions.

Table 2. Impact-Fatigue Results, AISI 310

T (K)	σ_A (10^3 psi)*	σ_F (10^3 psi)*	N	e (%)	RA (%)	RAN (%)	ϵ_E (%)	ϵ_T (%)	E_F (10^3 ft-lb/in^3)*
				Uniaxial, Annealed					
297	70.0	217.2	6,346	41	21	68	27	24	1.6
297	76.1	233.3	4,097	44	23	67	30	26	1.9
297	112.9	297.7	57	65	33	62	49	40	4.6
297	150.5	368.4	12	54	29	59	41	34	5.1
297	187.2	500.0	7	54	27	62	37	31	5.8
195	90.3	280.0	386	60	32	68	47	39	3.5
195	114.1	295.7	51	51	28	61	39	33	3.7
195	159.1	378.3	13	45	24	58	32	28	4.2
76	87.0	229.8	20,844	50	25	62	33	29	2.4
76	112.3	323.0	1,298	57	28	65	39	33	3.6
76	151.4	350.0	84	61	30	57	43	36	5.4
76	188.2	406.9	18	47	31	54	45	37	7.1
				Biaxial, Annealed					
297	53.8	81.0	4,897		34		52	42	2.3
297	60.5	86.8	3,809		30		43	36	2.2
297	75.7	137.3	501		45		82	60	5.2
297	112.3	205.9	8		45		82	60	7.7
195	74.5	117.6	869		37		59	46	3.7
195	100.0	154.1	39		35		54	43	4.5
195	113.5	187.5	9		39		64	49	6.1
195	201.1	327.1	1		39		64	49	10.7

76	74.4	97.9	4,992		24		32	28	2.0
76	89.8	115.9	1,892		18		22	20	1.6
76	114.1	145.8	30		22		28	25	2.7
76	153.0	212.1	6		28		34	29	3.5
Triaxial, Annealed									
297	40.1	43.4	2,138		8		9	9	0.3
297	52.5	61.8	889		15		18	17	0.8
297	57.4	67.7	645		15		18	17	0.9
297	78.8	105.9	14		26		35	30	2.3
195	38.0	38.3	5,991		1		1	1	0.03
195	52.6	53.5	1,684		2		2	2	0.1
195	87.7	98.6	429		11		12	11	0.9
76	53.0	54.0	2,518		2		2	2	0.1
76	83.9	89.8	238		7		8	8	0.6
76	111.5	120.7	33		8		9	9	0.8
Uniaxial, Strained 11% at 76 K									
297	78.7		61,300	23+	10+		11+	10+	0.7+
297	93.3	229.9	3,087	42	15	59	18	17	1.4
297	193.9	388.0	7	37	30	54	43	36	6.9
297	251.4	545.5	4	34	26	58	35	30	7.3
76	164.2	271.4	1,584	62	28	40	39	33	5.3
76	211.8	383.3	51	61	25	45	33	29	5.8

* 10^3 psi = 0.703 kg/mm^2

10^3 ft-lb/in^3 = 0.0828 joules/mm^3

\+ Fractured at grip

Table 3. Impact-Fatigue Results, AISI 304

T (K)	σ_A (10^3 psi)*	σ_F (10^3 psi)*	N	e (%)	RA (%)	RAN (%)	ϵ_E (%)	ϵ_T (%)	E_F (10^3 ft-lb/in^3)*
Uniaxial, Annealed									
297	71.8		24,500	42^+	28^+		39^+	33^+	2.3^+
297	90.8	224.0	10,340	39	39	59	64	49	4.8
297	75.3	189.1	9,300	97	42	60	72	54	4.5
297	106.6	329.0	930	71	36	68	56	44	5.0
297	123.8	379.2	100	114	45	67	82	60	8.5
297	137.3	411.7	54	65	34	67	52	42	5.9
297	106.1	304.3	45	100	40	65	67	51	5.9
297	143.6	378.3	14	70	36	62	56	44	6.7
297	172.4	500.0	9	68	78	66	61	48	8.8
195	100.9		12,000	18^+	14^+		16^+	15^+	1.3^+
195	148.7	383.5	35	42	21	61	27	24	3.4
195	135.2	335.2	23	40	13	60	15	14	1.7
76	111.1		10,270	14^+	10^+		11^+	10^+	1.0^+
76	137.9	286.0	1,548	32	18	52	22	20	2.5
76	173.3	315.3	435	35	21	45	27	24	3.9
76	266.7	500.0	19	38	24	47	32	28	7.1
Biaxial, Annealed									
297	54.4	72.1	4,061		24		32	28	1.5
297	59.6	90.3	975		35		54	43	2.7
297	75.3	147.3	58		49		96	67	6.0
297	131.4	261.0	6		50		100	69	11.0
297	112.3	214.2	6		48		92	65	8.6

195	81.5	91.1	2,615	11	12	11	0.8
195	98.4	136.8	676	28	39	33	3.2
195	120.7	189.2	128	36	56	44	4.6
195	156.4	250.0	17	37	59	46	7.7
76	76.3	82.8	4,149	8	9	9	0.6
76	82.3	86.0	2,073	4	4	4	0.3
76	85.7	91.3	1,227	6	6	6	0.4
76	104.3	121.7	569	14	16	15	1.4
76	108.2	128.8	132	16	19	17	1.7
76	138.6	172.8	57	20	25	22	2.9
76	176.8	222.9	9	21	27	24	4.0
Triaxial, Annealed							
297	43.5	50.1	5,568	13	15	14	0.5
297	58.0	68.0	955	15	18	17	0.9
297	105.9	208.8	13	49	96	67	8.5
195	52.9	55.5	3,454	5	5	5	0.2
195	70.1	71.3	1,231	2	2	2	0.1
195	89.2	120.0	644	26	35	30	3.6
76	53.0	55.1	3,156	4	4	4	0.2
76	87.5	92.7	458	6	6	6	0.4
76	135.0	156.1	72	14	16	15	1.8

Table 3. Impact-Fatigue Results, AISI 304 (continued)

T (K)	σ_A (10^3 psi)*	σ_F (10^3 psi)*	N	e (%)	RA (%)	RAN (%)	ϵ_E (%)	ϵ_T (%)	E_F (10^3 ft-lb/in^3)*
Uniaxial, Precycled to 76 K									
297	89.8	262.5	491	44	25	66	33	29	2.5
297	137.9	388.8	16	61	30	65	43	36	4.9
76	139.3	286.0	7,521	28	18	51	22	20	2.6
76	228.1	347.1	15	32	19	34	23	21	4.4
Biaxial, Precycled to 76 K									
297	42.6	50.0	10,340		15		18	17	0.6
297	58.3	86.8	1,279		32		47	39	2.3
297	74.9	130.8	109		43		75	56	4.7
297	94.8	155.6	16		39		64	50	5.1
76	105.0	198.1	247		47		89	64	7.8
76	157.3	207.4	90		23		30	26	3.9
Uniaxial, Sensitized at 1000° F									
297	83.7	183.3	10,506	80	42	54	72	54	5.0
297	114.1	428.5	38	73	39	73	64	49	6.1
76	131.5		11,255	18^+	13^+		15^+	14	1.6^+
76	190.2	315.3	104	32	21	40	27	24	4.3

			Uniaxial, Welded						
297	60.5	114.2	11,518	35		47			
297	90.3	215.4	67	36		53			
297	112.9	323.0	31	57		65			
195	84.6	205.0	8,818	44		59			
195	105.3	222.7	1,780	55		53			
195	127.3	353.6	33	46		81			
195	189.2	406.9	7	46		54			
76	114.1	153.3	9,200	34		26			
76	151.3	291.0	584	46		48			
76	188.1	388.0	20	47		52			
			Biaxial, Welded (Notch at Weld)						
297	44.9	54.9	6,446		18		22	28	0.8
297	59.3	94.1	1,137		37		59	46	2.9
297	89.8	150.0	11		40		67	51	5.0
76	59.6	72.3	3,888		18		22	20	1.1
76	89.8	120.9	269		26		35	30	2.6
76	149.7	241.4	10		38		61	48	7.6

Table 3. Impact-Fatigue Results, AISI 304 (continued)

T (K)	σ_A (10^3 psi)*	σ_F (10^3 psi)*	N	e (%)	RA (%)	RAN (%)	ϵ_E (%)	ϵ_T (%)	E_F (10^3 ft-lb/in^3)*
Biaxial, Welded (Notch 1/16'' from Weld)									
297	52.1	67.6	3,184		23		30	26	1.3
297	75.3	127.3	92		41		69	52	4.3
76	67.7	94.7	2,620		28		39	33	2.2
76	149.7	274.5	5		45		82	60	10.2
Biaxial, Welded (Notch 1/8'' from Weld)									
297	52.1	70.5	2,435		26		35	30	1.5
297	75.3	120.7	26		38		61	47	3.8
76	67.7	74.1	2,875		9		10	10	0.6
76	134.8	193.8	8		30		43	36	4.8
Uniaxial, Strained 11% at 76 K									
297	120.4	172.3	6,844	29	11	30	12	11	1.2
297	170.7		128	25^+	9^+		10^+	10^+	1.4^+
297	265.8	552.6	10	40	12	52	14	13	3.1
76	202.4	381.8	1,456	34	10	47	11	10	1.9
76	256.1	482.8	177	37	9	47	10	10	2.1
76	345.7	495.6	10	33	10	30	11	10	3.2

* 10^3 psi = 0.703 kg/mm^2
10^3 ft-lb/in^3 = 0.0828 joule/mm^3
\+ Fractured at grip

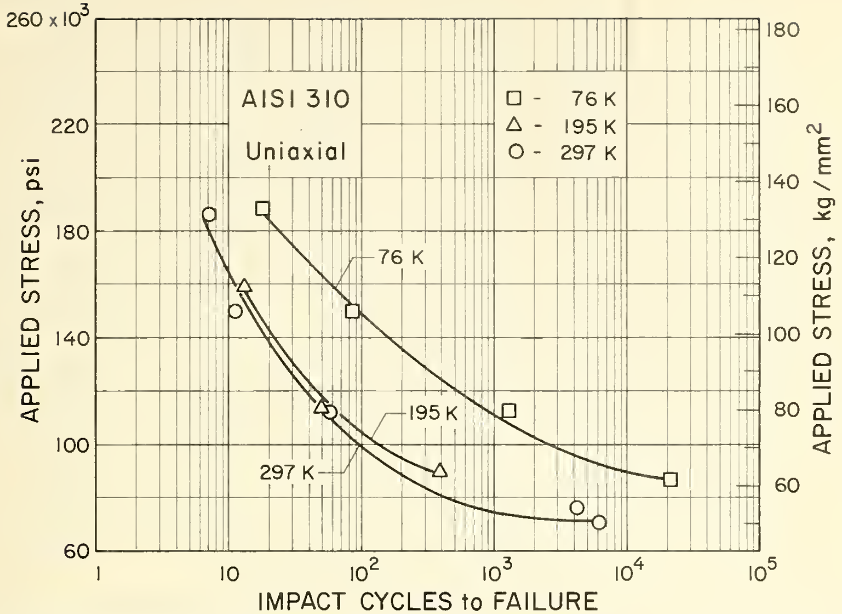

Figure 4. S-N curve for AISI 310, uniaxial.

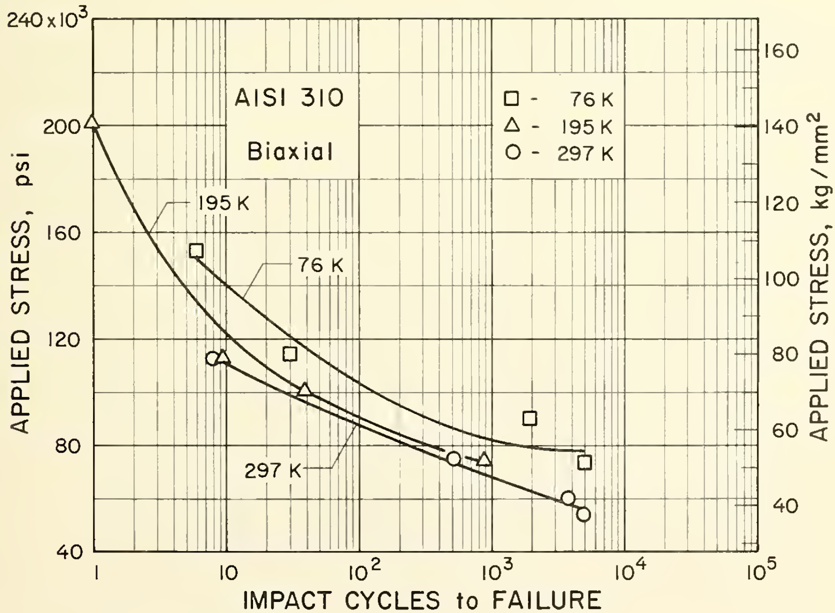

Figure 5. S-N curve for AISI 310, biaxial.

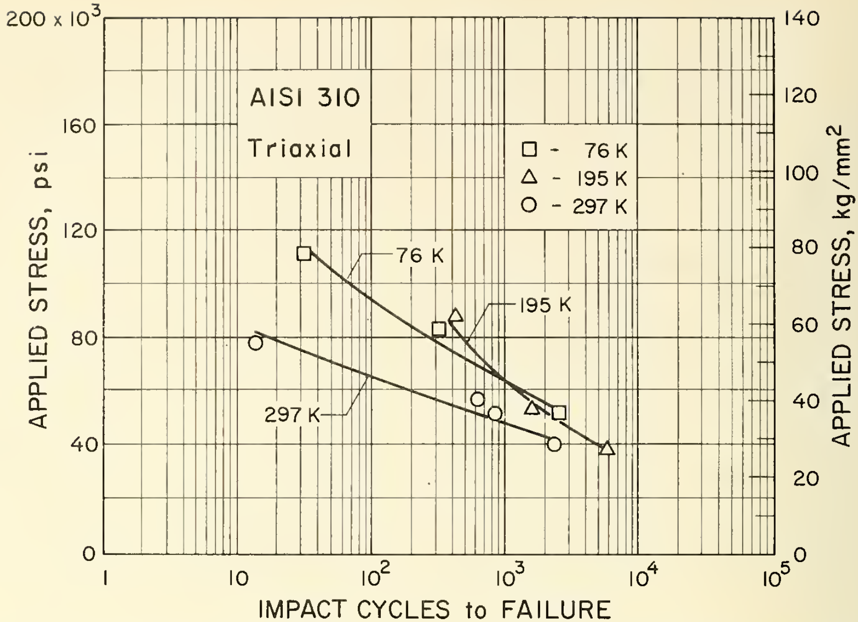

Figure 6. S-N curve for AISI 310, triaxial.

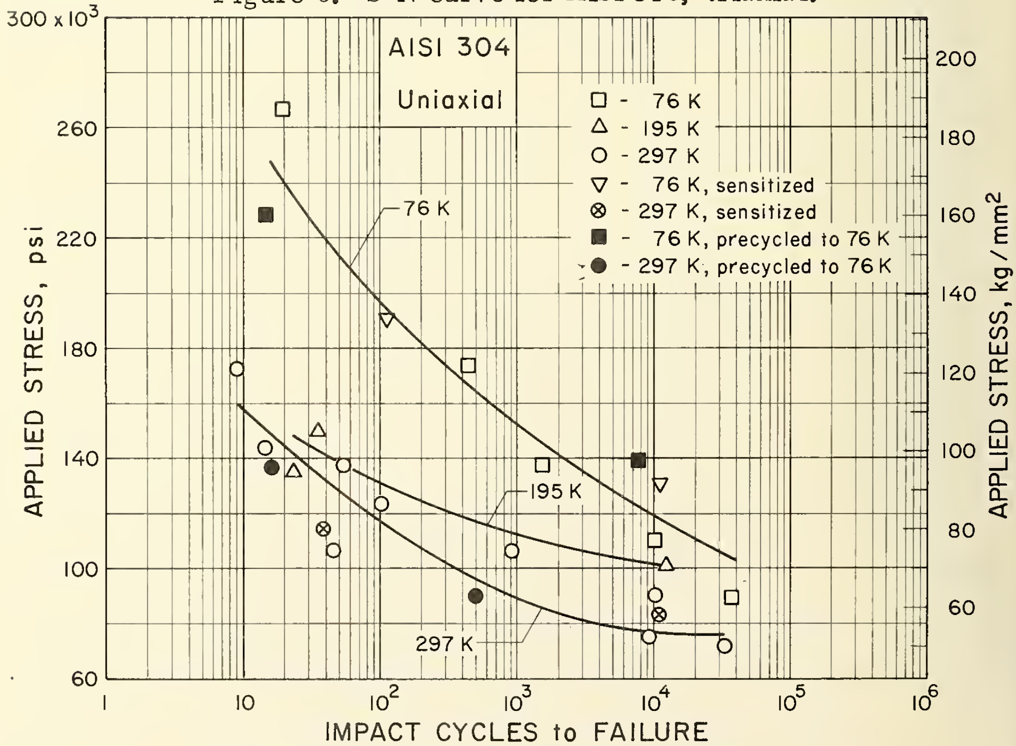

Figure 7. S-N curve for AISI 304, uniaxial.

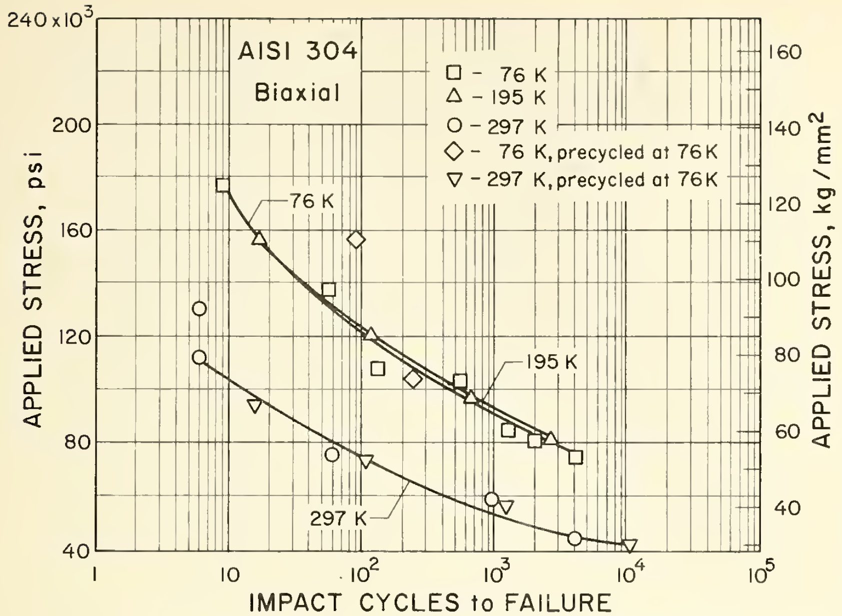

Figure 8. S-N curve for AISI 304, biaxial.

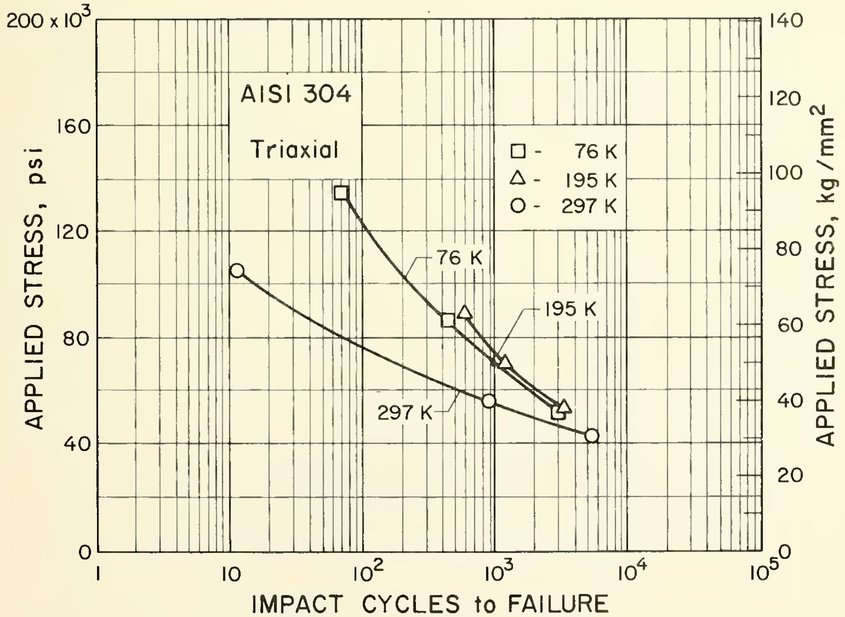

Figure 9. S-N curve for AISI 304, triaxial.

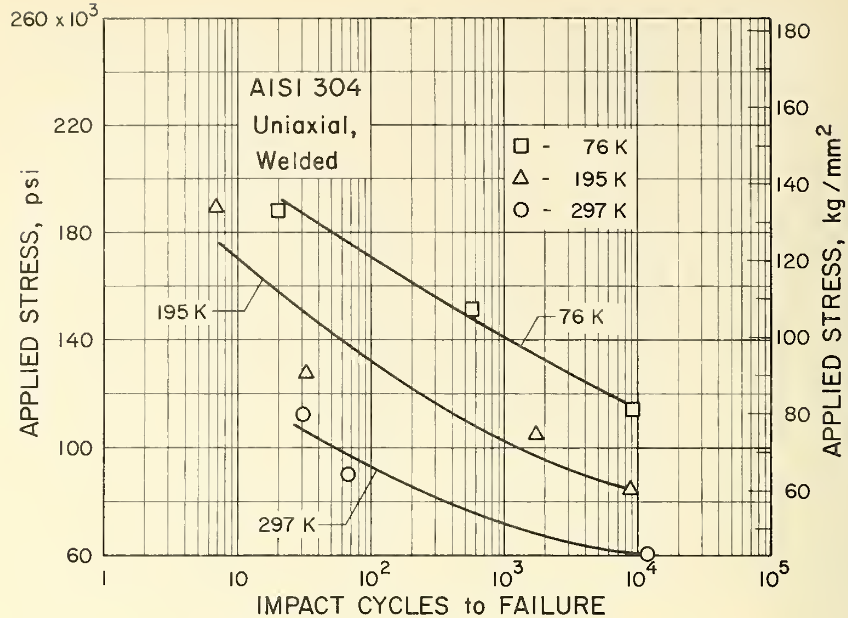

Figure 10. S-N curve for AISI 304, uniaxial, welded.

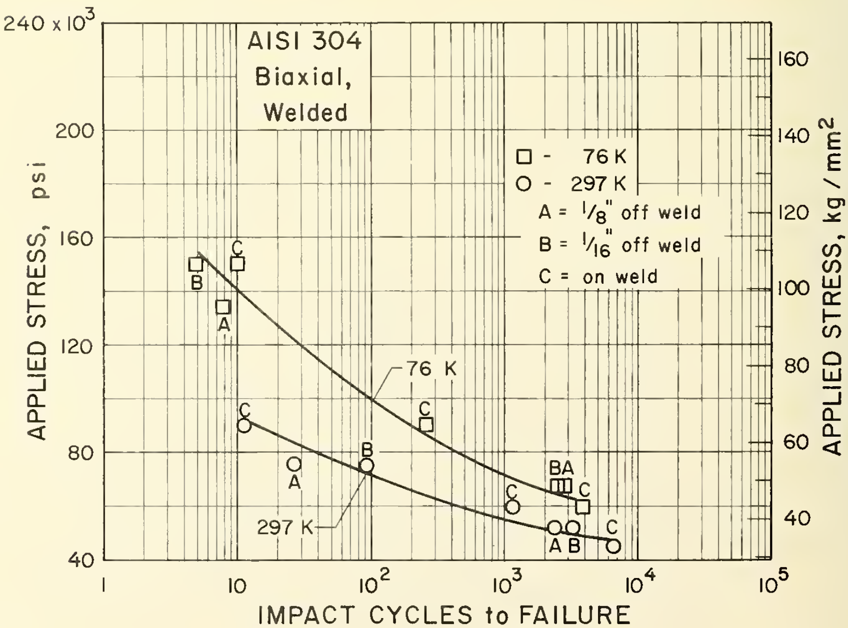

Figure 11. S-N curve for AISI 304, biaxial, welded.

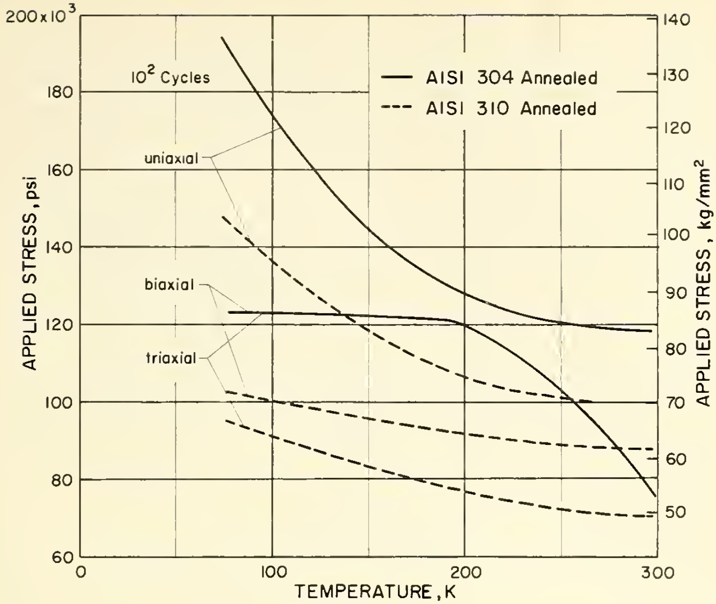

Figure 12. Fatigue life at 10^2 cycles.

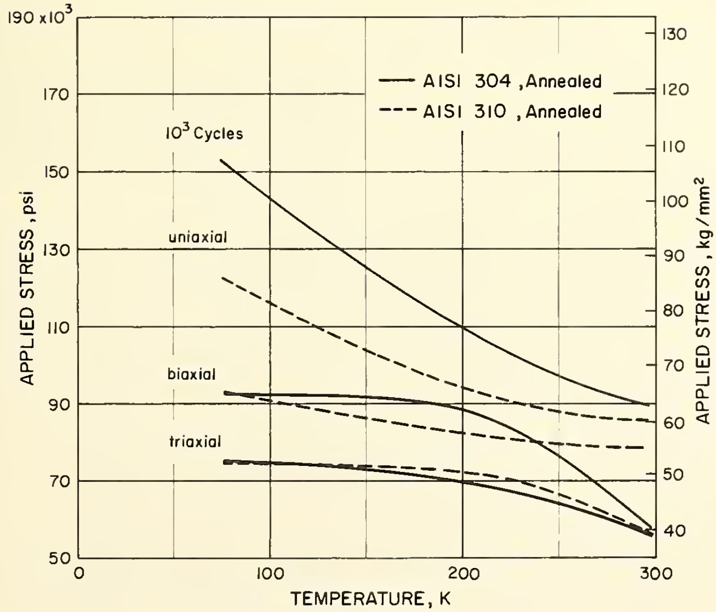

Figure 13. Fatigue life 10^3 cycles.

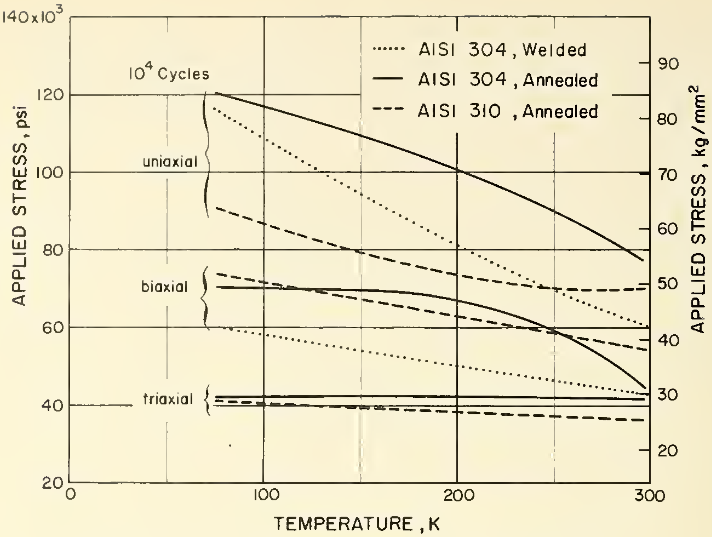

Figure 14. Fatigue life at 10^4 cycles.

Figure 15 allows comparison with some previous fatigue life measurements[15-19] that were conducted in tension-compression. While the impact and conventional fatigue curves do have the same general structure, there are some differences:

(1) The impact S-N curves fall at a higher stress level.

(2) The fatigue limit on impact, uniaxial stress appears to occur at or above the yield strength (0.002 offset) as determined from tensile tests; in conventional fatigue the limit is well below this level.

These factors are probably related to the increase in yield strength with increasing strain rate.

Data from the literature[20-22] show that cold-work has a significant effect on the mechanical properties of 18 Cr-8 Ni steels, and Figures 15 and 16 show this effect on fatigue life. To make a controlled

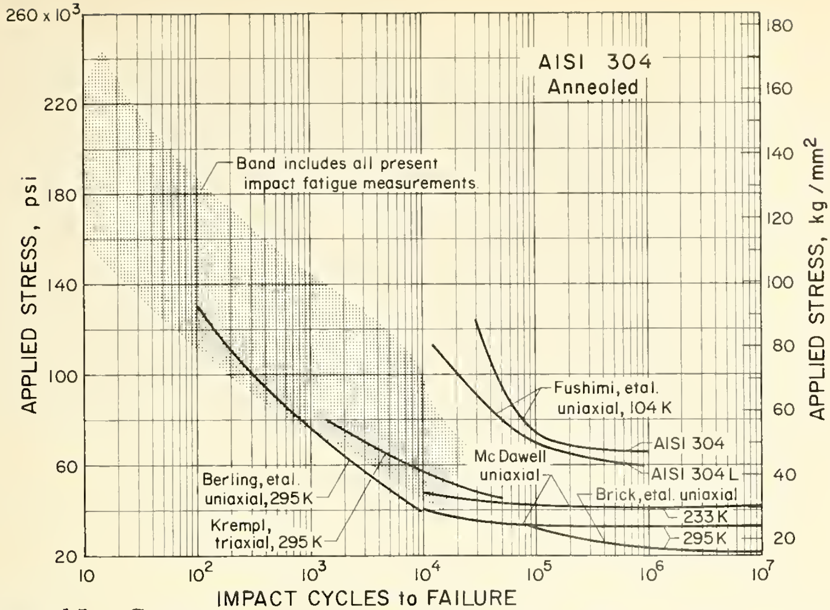

Figure 15. Comparison of impact-fatigue data for annealed AISI 304 with that obtained in tests using tension-compression at low strain rates (Refs. 15-19). The triaxial samples of Krempl[17] had a stress concentration factor, K_t, of 3.3.

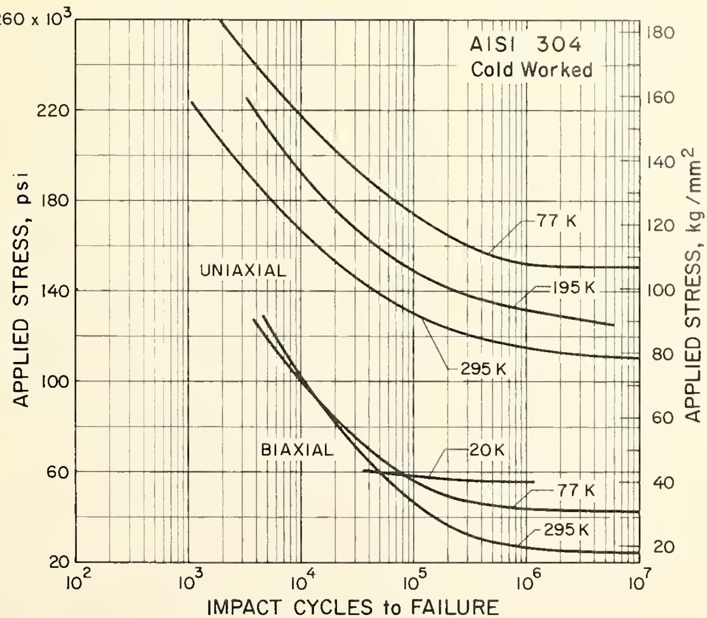

Figure 16. Fatigue-life data (Ref. 20-22) for cold-worked (to 210,000 psi tensile strength) AISI 304. Tests were conducted by tension-compression at low strain rates. The biaxial samples had a stress concentration factor, K_t, of 2.75 to 3.9.

check of the effect of cold-work on 304 and 310, uniaxial specimens were strained 11%, as noted above, and then impacted in the usual manner. Figure 17 shows the results and comparison with Figures 4 and 7 indicates a considerable strengthening at both 297 and 76K. At a life of 10^3 cycles, the improvement in the applied stress is about 40-50%. Also, the superiority of AISI 304 over 310 is again evident.

Figures 18-25 show that the fracture stress for all materials and all configurations follows a pattern very similar to the applied stress with two exceptions:

(1) The 310 biaxial data (Figure 19) lie on a single curve for all temperatures.

(2) The 304 biaxial data (Figure 22) show a small separation between the precycled and annealed room temperature curves.

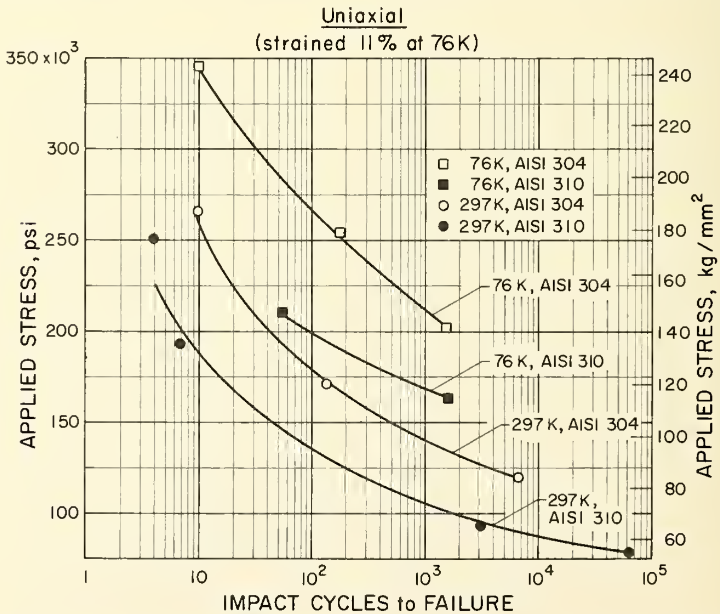

Figure 17. Impact-fatigue data for cold-worked uniaxial specimens. The 304 contained 50% martensite after straining.

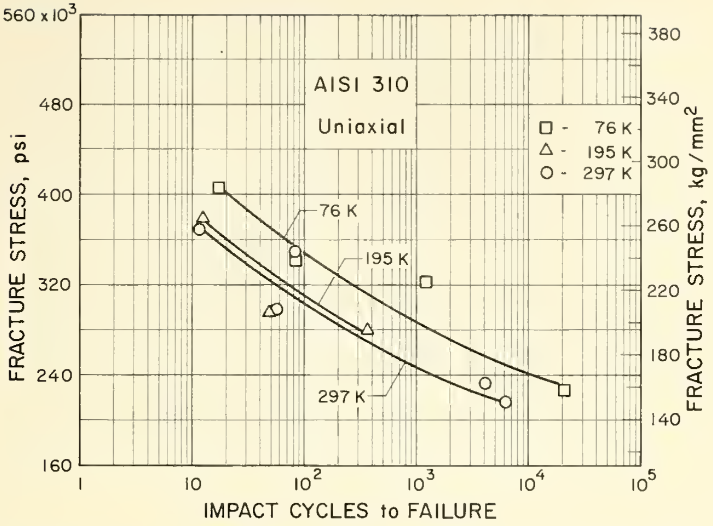

Figure 18. Fracture stress for AISI 310, uniaxial.

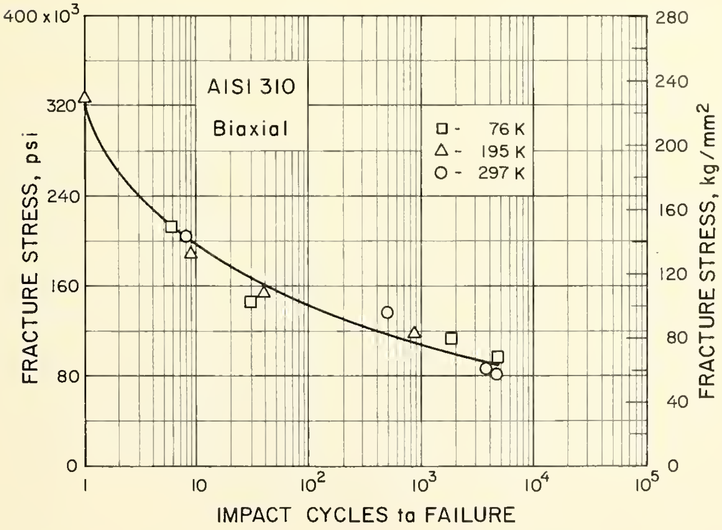

Figure 19. Fracture stress for AISI 310, biaxial.

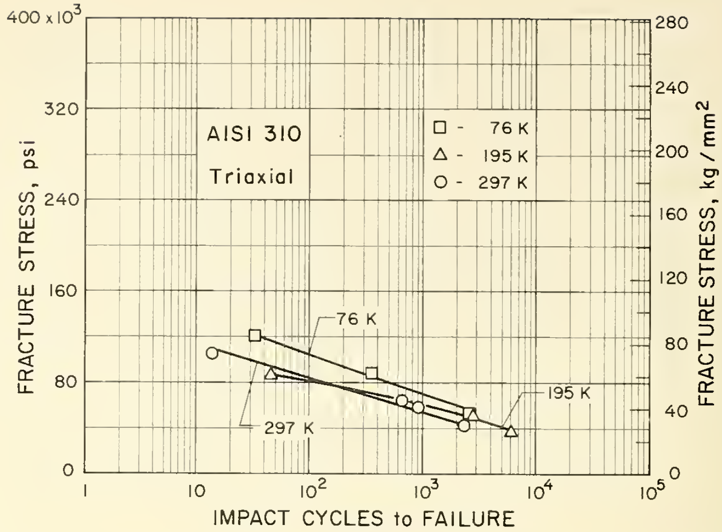

Figure 20. Fracture stress for AISI 310, triaxial.

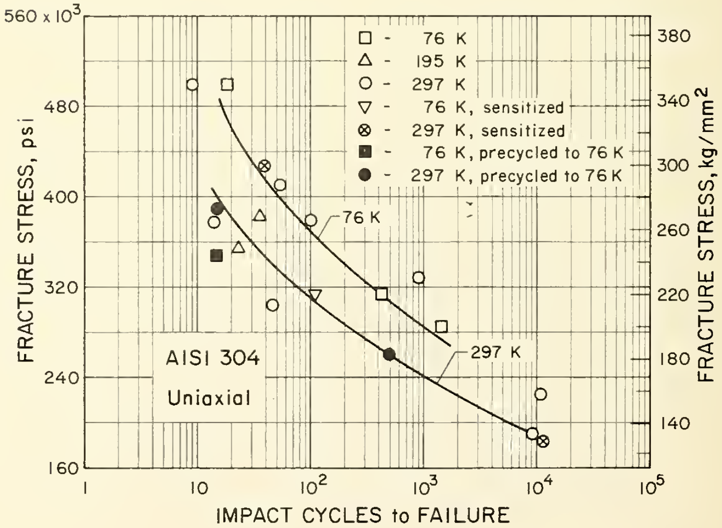

Figure 21. Fracture stress for AISI 304, uniaxial.

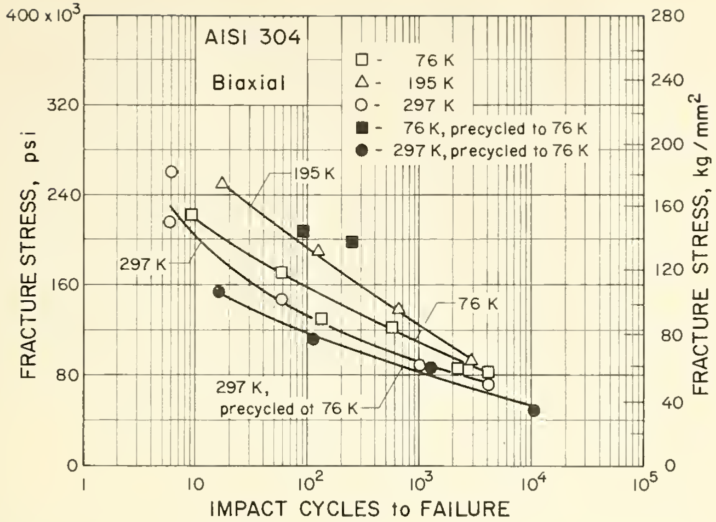

Figure 22. Fracture stress for AISI 304, biaxial.

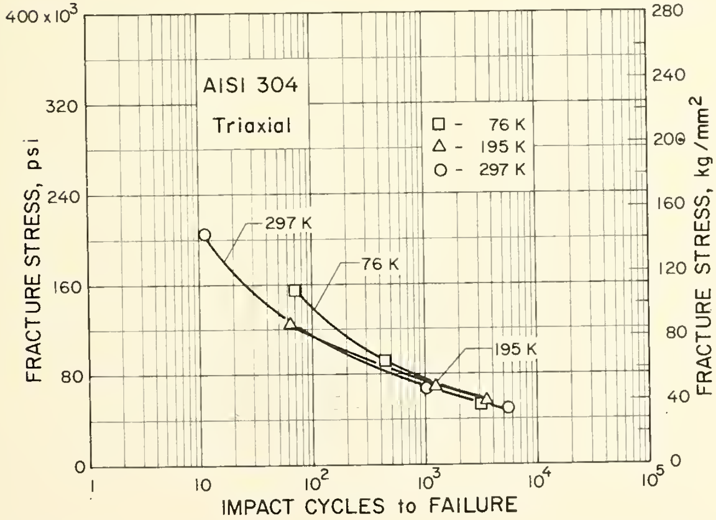

Figure 23. Fracture stress for AISI 304, triaxial.

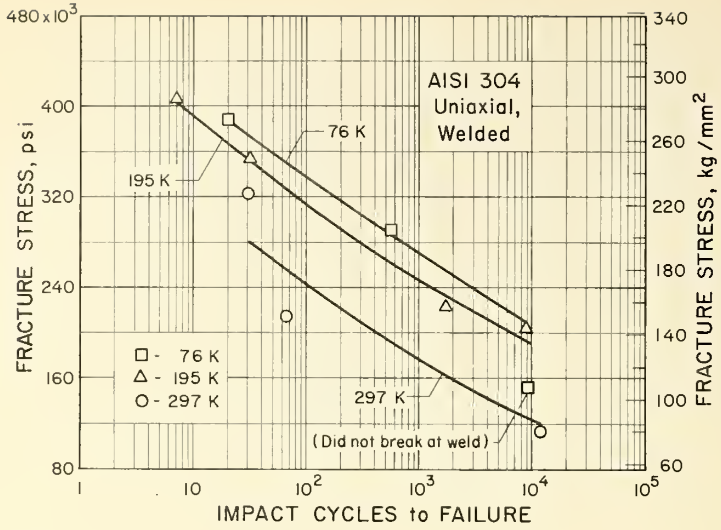

Figure 24. Fracture stress for AISI 304, uniaxial, welded.

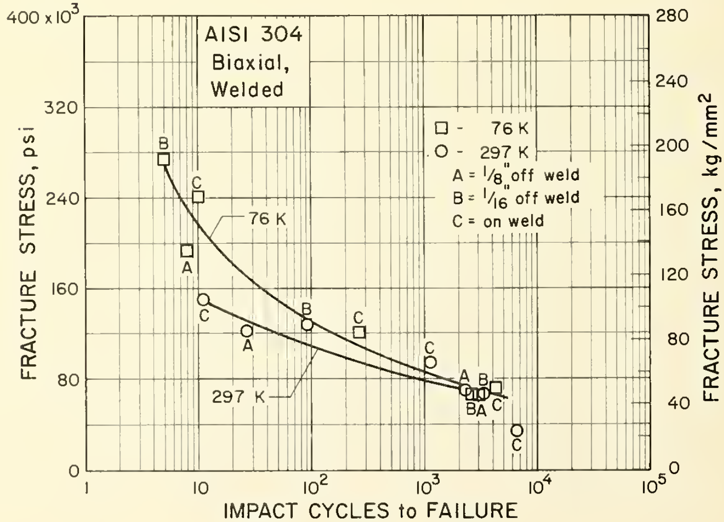

Figure 25. Fracture stress for AISI 304, biaxial, welded.

Another technique to characterize the mechanical behavior is to consider the applied energy needed to fracture specimens. This may be considered, to a first approximation, as the product of the applied stress and specimen strain (A more detailed approximation is described in Section 4 and used in all calculations). This computed deformation energy density, E_F, is plotted versus the log of the number of cycles to failure, N, in Figures 26-32. In the range tested, these curves can be approximated by an exponential relation,

$$N = N_0 \exp\left(\frac{-mE_F}{kT}\right),$$

between the number of cycles to failure, N, and E_F, where N_0 and m are material constants for a given stress configuration and k is Boltzmann's constant. In all but one case, the amount of energy that must be absorbed by the sample before fracturing decreases with the temperature. The one exception to this decrease in absorbed energy with temperature is the AISI 310 uniaxial (Figure 26). Figures 29 and 30 indicate that the presence of martensite in AISI 304 prior to testing decreases the energy absorbed before fracture. The relative position of weld and notch has very little effect on absorbed energy at 297K, but does exert a considerable influence at 76K (Figure 32). Figure 33 displays summary curves at 10^3 cycles and the deviation of the AISI 310 uniaxial is obvious.

The ductile behavior of the two steels can be seen in Figures 34 and 35. Again, the room temperature differences are small but increase considerably as the temperature decreases. The low ductility of AISI 304 at 76K is probably due to the large amount of martensite present.

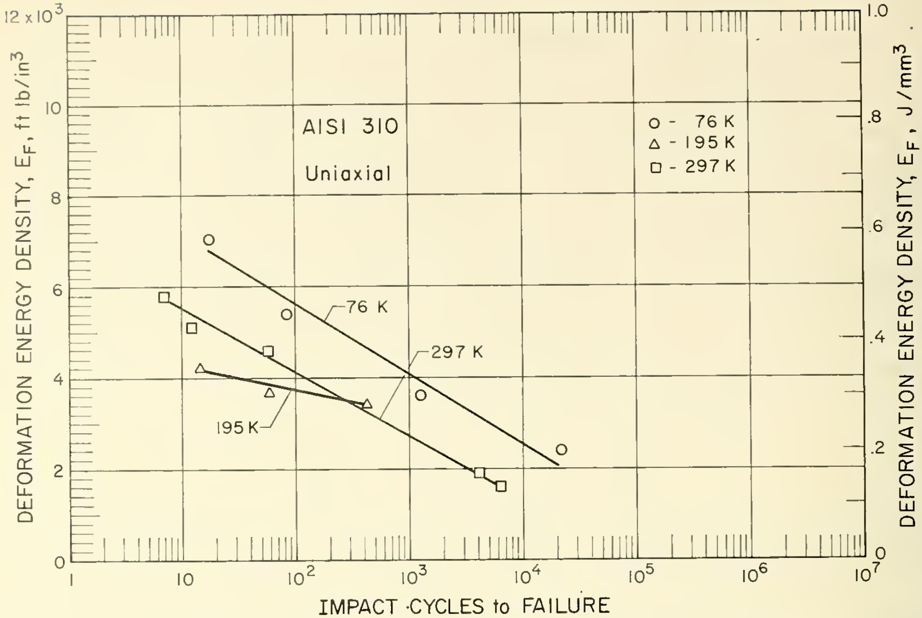

Figure 26. Deformation energy density for fracture of AISI 310, uniaxial.

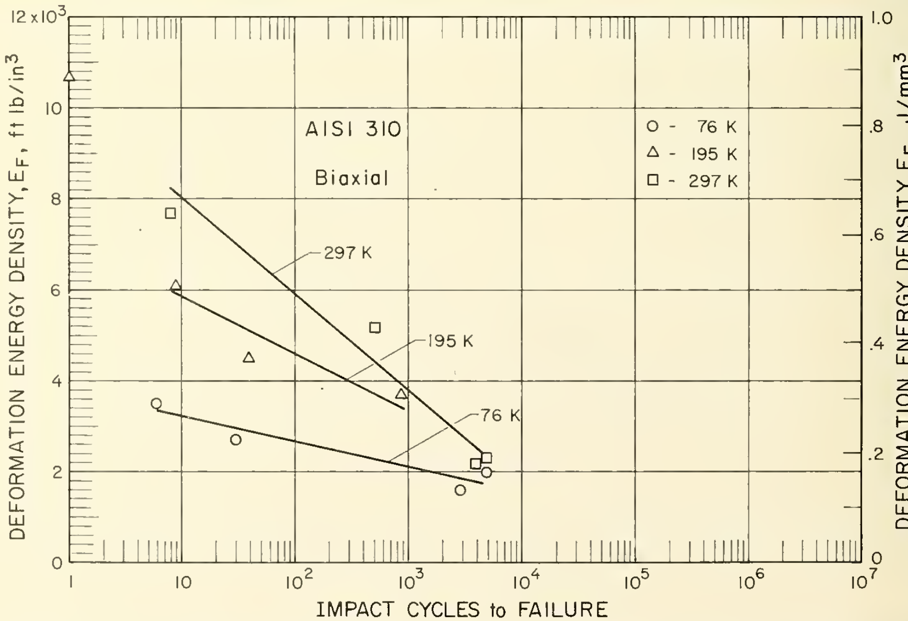

Figure 27. Deformation energy density for fracture of AISI 310, biaxial.

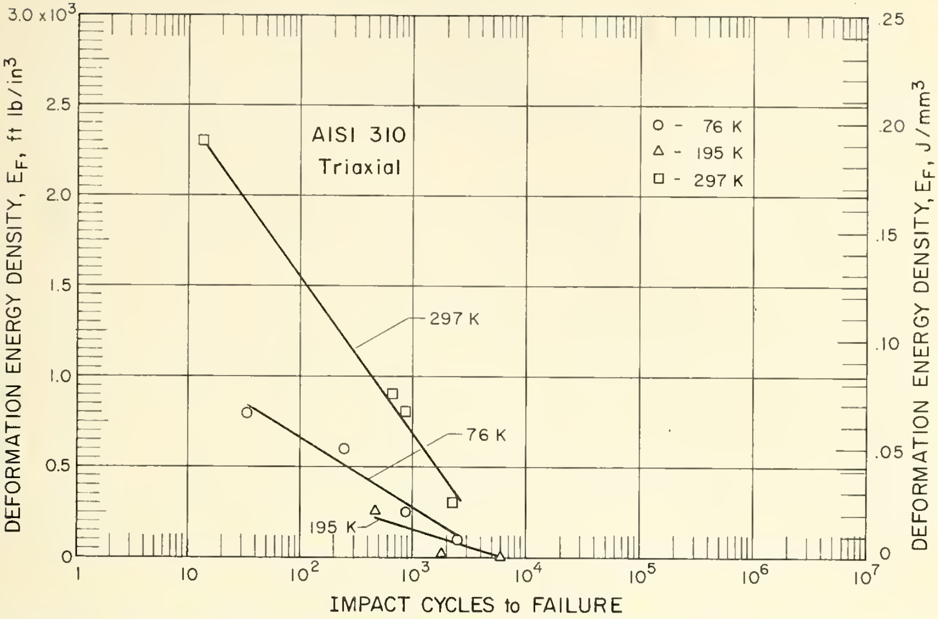

Figure 28. Deformation energy density for fracture of AISI 310, triaxial.

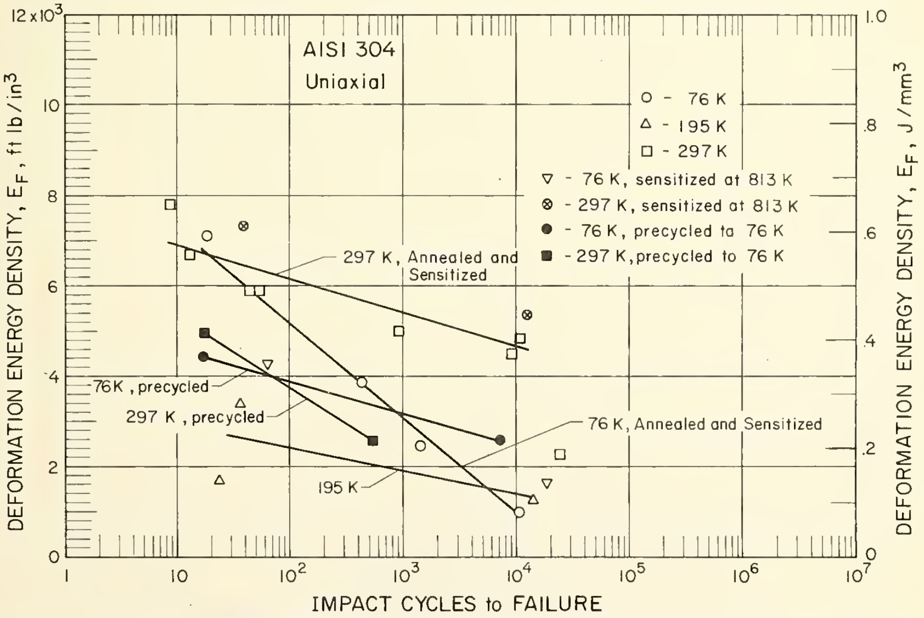

Figure 29. Deformation energy density for fracture of AISI 304, uniaxial.

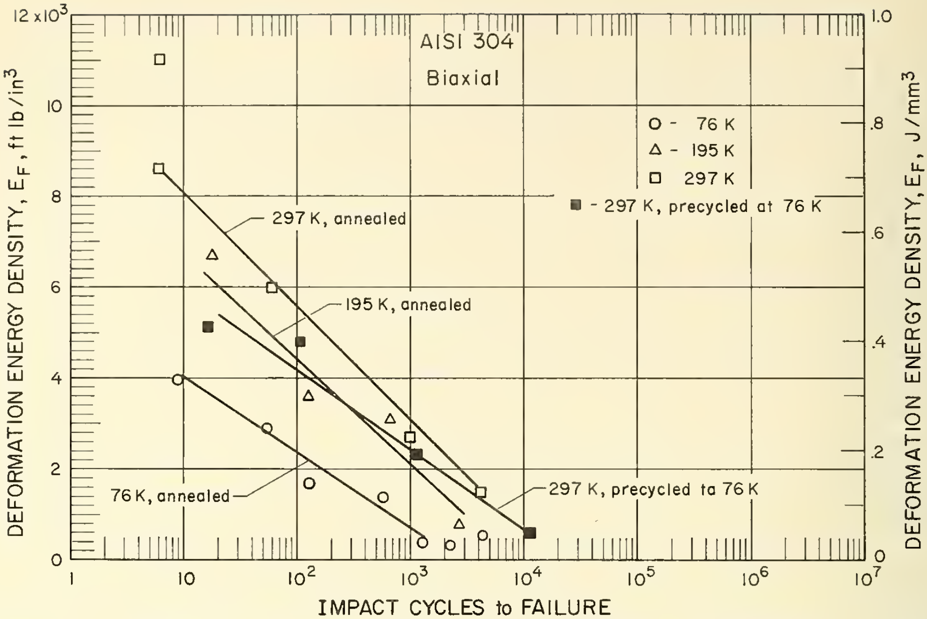

Figure 30. Deformation energy density for fracture of AISI 304, biaxial.

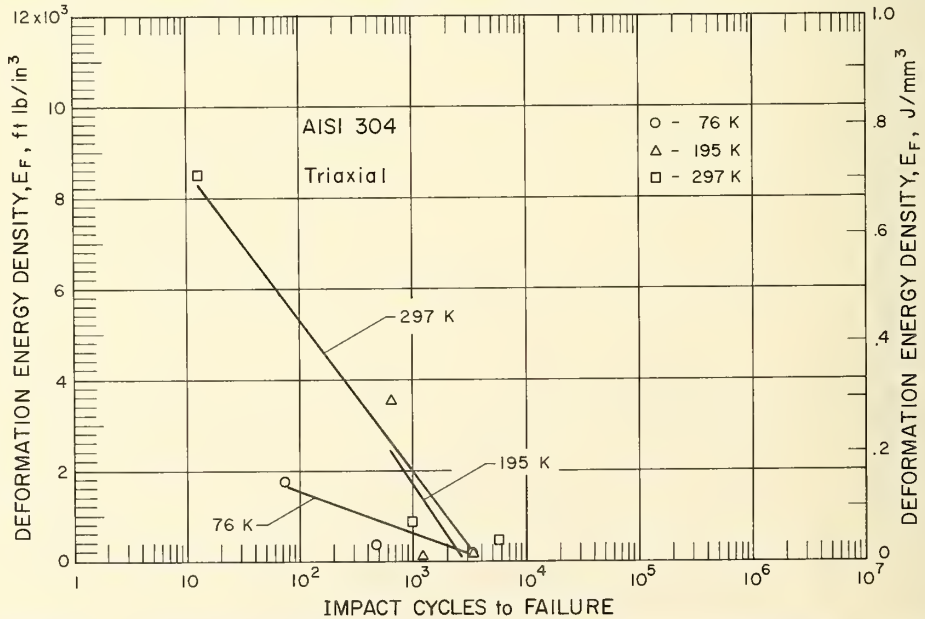

Figure 31. Deformation energy density for fracture of AISI 304, triaxial.

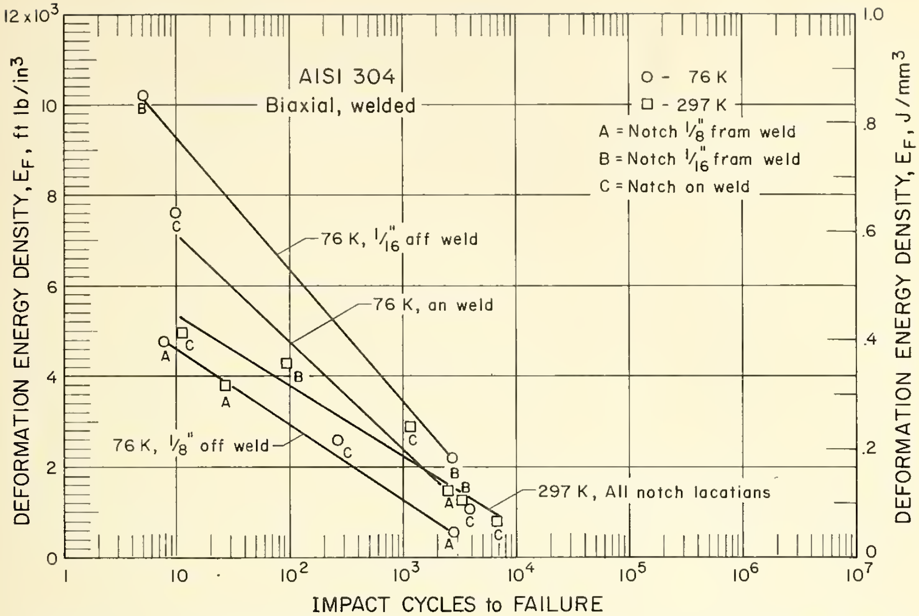

Figure 32. Deformation energy density for fracture of AISI 304, biaxial, welded.

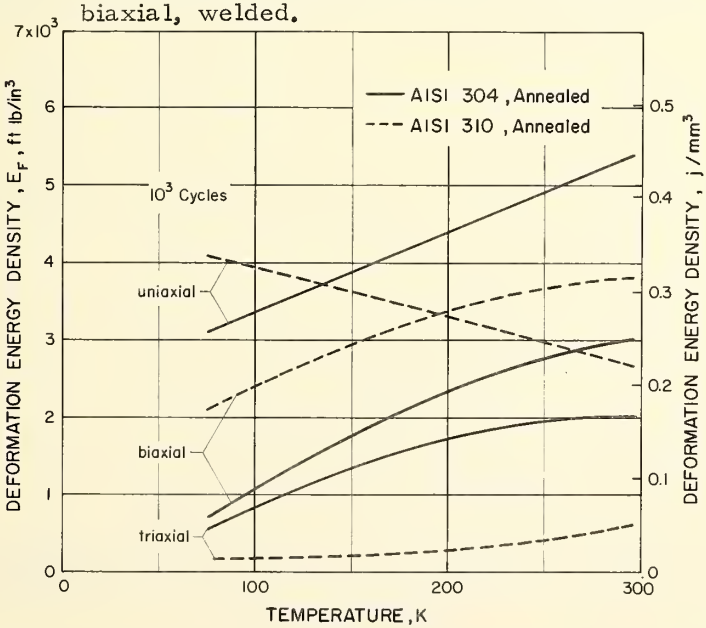

Figure 33. Summary of deformation energy density for fracture at 10^3 cycles.

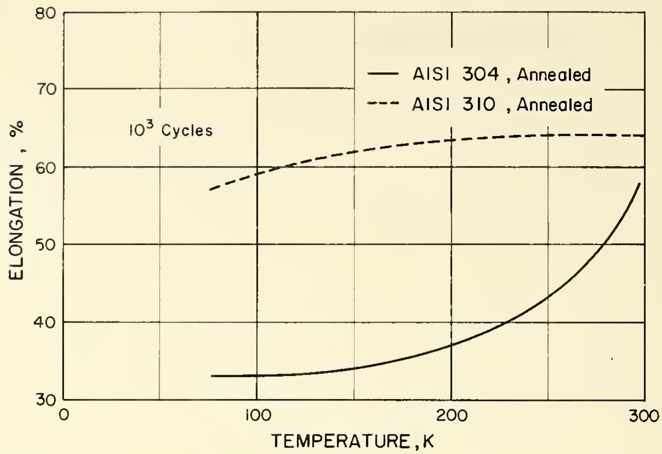

Figure 34. Elongation in one inch for fracture at 10^3 cycles.

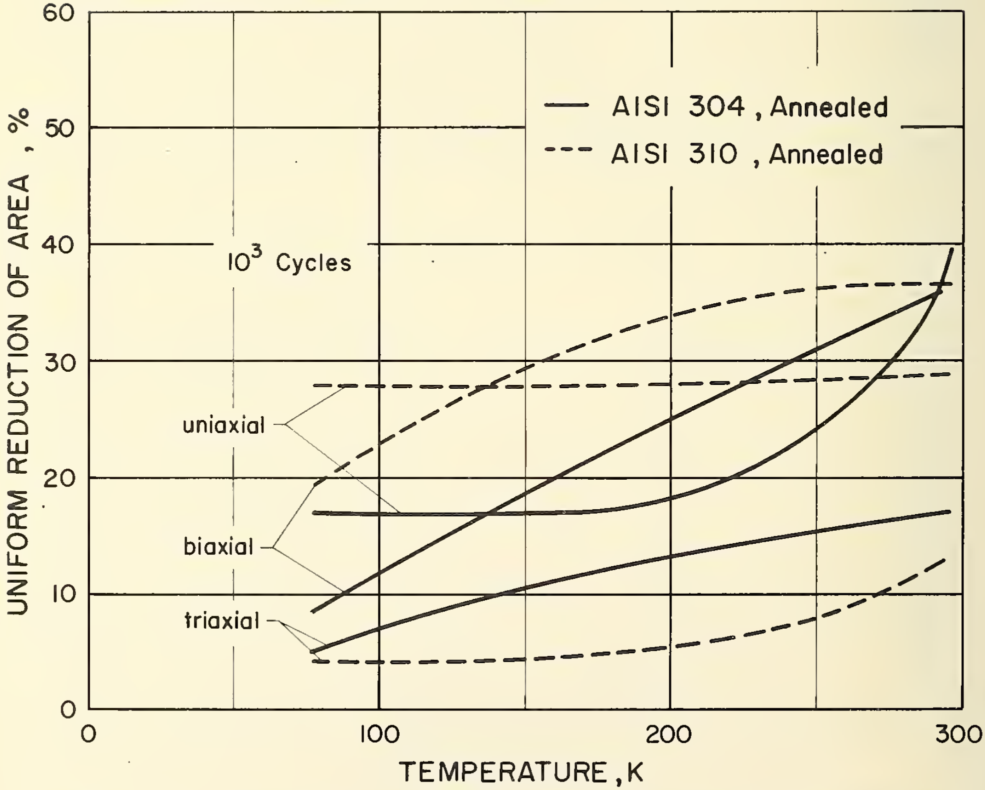

Figure 35. Uniform reduction of area for fracture at 10^3 cycles.

The progress of one impact test on a uniaxial 304 specimen at 297K was interrupted frequently to make measurements on the elongation, reduction of area, and amount of martensite formed. From the results in Figure 36, it appears that all three quantities reach a plateau and then increase abruptly before fracture.

5.2 Mechanical--Tensile

The results of the tensile tests on both steels are presented in Table 4. The sample elongation shows that the ductility does decrease as the strain rate increases. The considerable increase in yield strength noted for the moderate strain rate of 20 min^{-1} may possibly be due to a response time in the strip chart recorder too low to properly follow the load extension curve at this higher crosshead speed.

The inverse relationship between strain rate and ductility has been observed previously.[9,11,23] An increasing strain rate has also

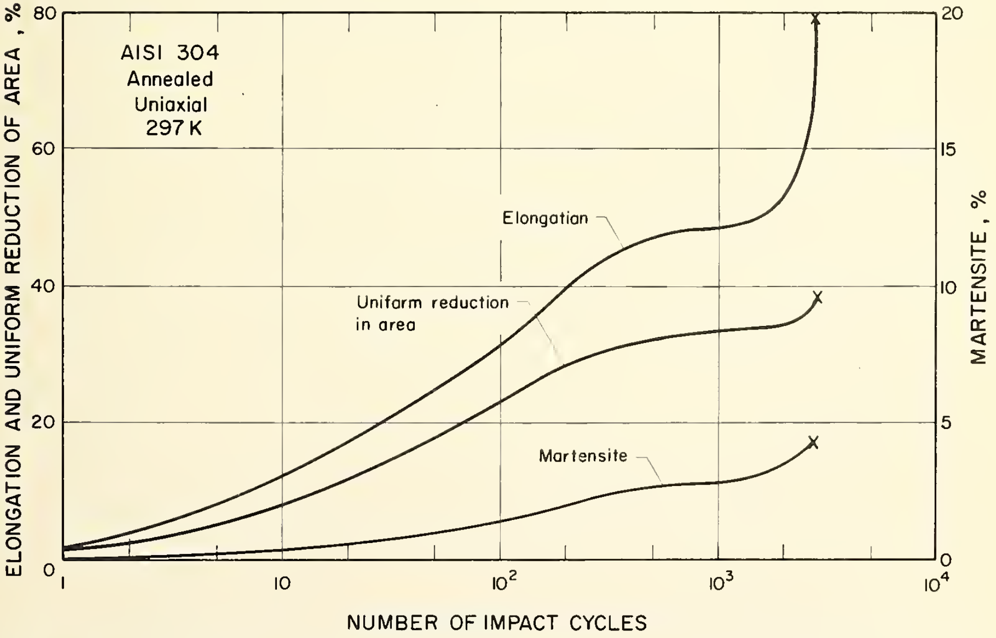

Figure 36. Parameters during an impact-fatigue test of AISI 304 at 297 K.

Table 4. Tensile Results.

AISI Type	Configuration	T (K)	$\dot{\epsilon}$ (min^{-1})	σ_Y (.002) (10^3 psi)*	σ_U (10^3 psi)*	σ_F (10^3 psi)*	E (10^6 psi)*	e (%)	RA (%)	RAN (%)	ϵ_ϵ (%)	ϵ_T (%)
304	uniaxial	297	0.002	38.9	100.0	357.1	29.5	79	46	72	85	62
304	uniaxial	297	0.2	38.8	92.5	355.8	27.5	58	34	74	52	42
304	uniaxial	297	20.	76.3†	94.7	263.1		44	25	64	33	29
304	uniaxial	76	0.002	49.1	190.2	432.3	25.3	41	27	56	37	31
304	uniaxial	76	0.2	53.5	203.5	407.0	23.9	38	18	50	22	20
304	uniaxial	76	20.	102.7†	193.6	420.9		32	22	54	28	25
304	uniaxial	76	20.	119.5†	208.0	442.6		32	19	53	23	21
310	uniaxial	297	0.002	38.0	93.3	282.7	29.9	42	19	67	23	21
310	uniaxial	297	0.2	38.0	89.7	249.2	28.2	43	22	64	28	25
310	uniaxial	297	20.	73.9†	90.4	226.0		41	22	60	28	25
310	uniaxial	76	0.002	84.4	178.2	396.0	37.3	69	36	55	56	44
310	uniaxial	76	0.2	88.8	185.0	420.5	36.8	70	38	56	61	48
310	uniaxial	76	20.	133.7†	163.1	332.9		31	21	51	27	24
304	uniaxial, welded	297	0.02	49.5	85.8‡	209.3	38.8			59		
304	uniaxial, welded	76	0.02	77.1	203.2‡	635.0	34.2			68		
304	biaxial	297	0.02		109.6	283.3			54		117	77
304	biaxial	195	0.02		185.4	289.7			36		56	44
304	biaxial	76	0.02		274.3	370.7			26		35	30
310	biaxial	297	0.02		103.5	188.2			45		82	60
310	biaxial	195	0.02		121.0	201.7			40		67	51
310	biaxial	76	0.02		171.8	245.4			30		43	36

* 10^3 psi = 0.708 kg/mm^2

† These values are perhaps too high, see text for further discussion.

‡ Fractured in weld.

been shown to decrease the amount of material transformed in metastable alloys.[3,9,24,25] In turn, the amount of martensite has been related directly to the tensile and yield strengths of the metal; generally they increase together.[26] As would be expected from these two observations, the tensile strength will tend to decrease as the strain rate is increased.[9]

True stress-true strain curves for both alloys have been recorded in Figures 37 and 38. These were constructed from the load-extension curve obtained during the tests, with the assumption that the elongation is equal to the engineering strain; this assumption should be valid until necking occurs shortly before fracture. The spread of some representative tensile test data[5, 27-29] is shown in Figures 39 and 40, and the present data show general agreement with these results with the exception of the yield strength at 20 min^{-1} as noted above.

5.3 Transformation Products in AISI 304

The amount of martensite transformation product formed in 304 is a function of strain, strain rate, temperature, and chemical composition. The amount of bcc phase present is most easily determined by measuring relative magnetic permeability. This can be performed quite rapidly with a Magne-Gage, a device which measures the force required to pull a standard magnet from the surface of the sample. Using this technique, careful observations have been made previously on transformed martensite during the progress of tensile tests.[5] In a similar manner, as noted above, we recorded measurements for an AISI 304 annealed, uniaxial sample during its impact-fatigue life at 297K. Figure 41 indicates that, as in tensile tests, the percent martensite increases with the strain. In this same figure, point data are included from measurements on samples after being impacted to fracture. In general, the results at room temperature

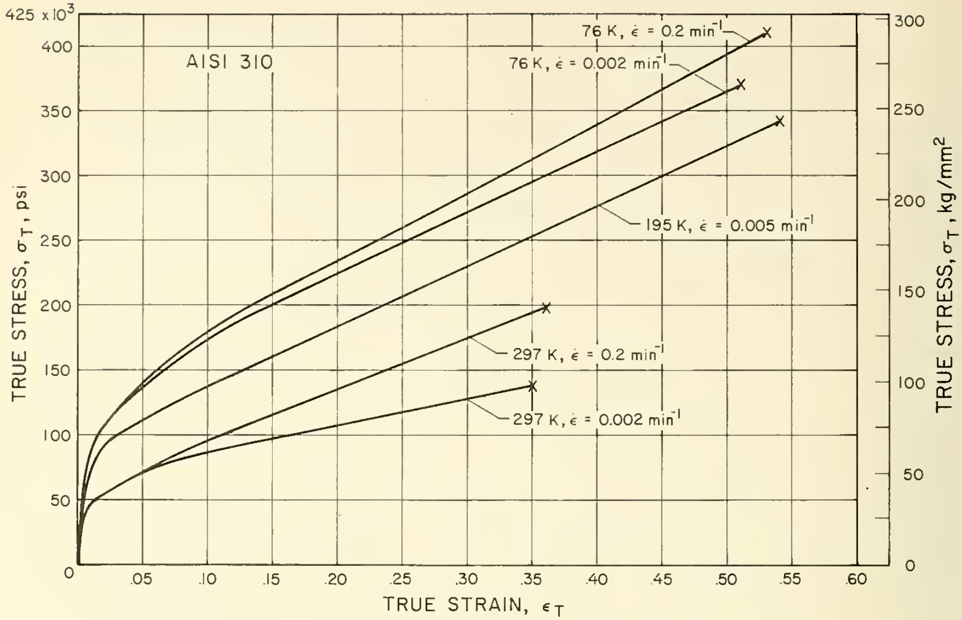

Figure 37. True stress-true strain curves for tensile tested AISI 310.

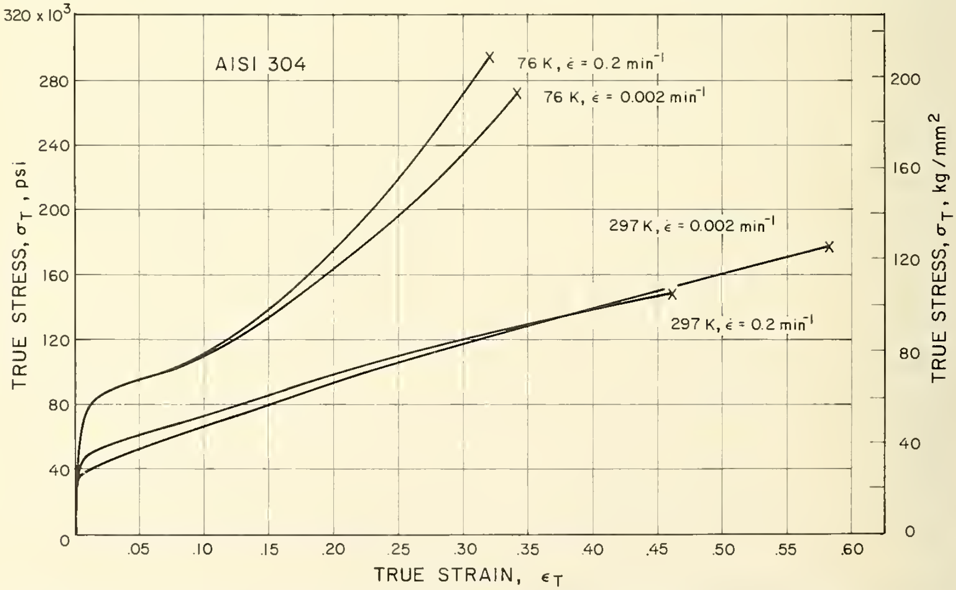

Figure 38. True stress-true strain curves for tensile tested AISI 304.

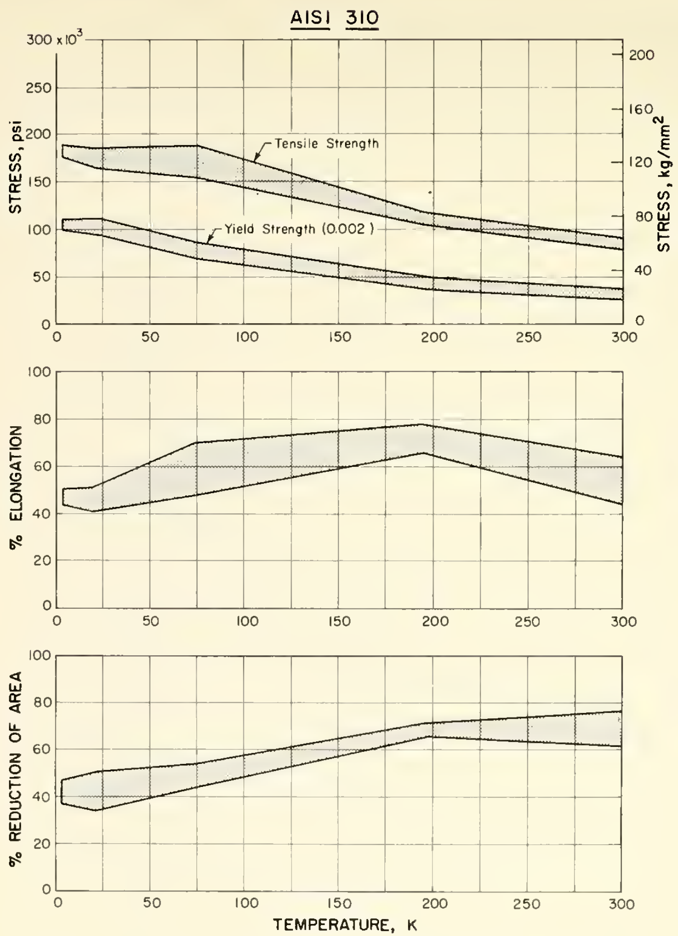

Figure 39. Representative tensile test data for annealed AISI 310.

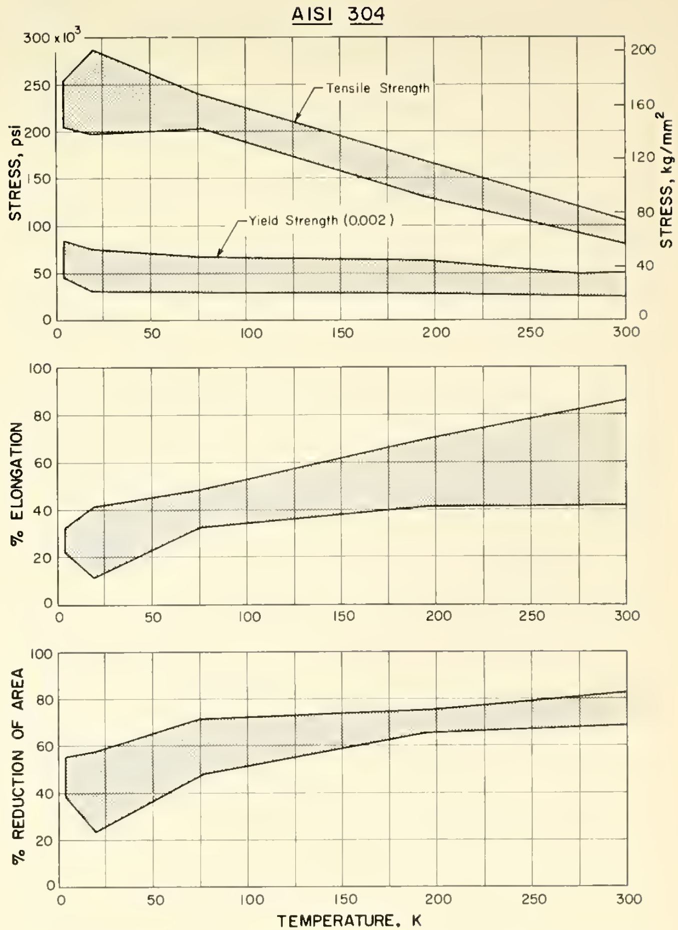

Figure 40. Representative tensile test data for annealed AISI 304.

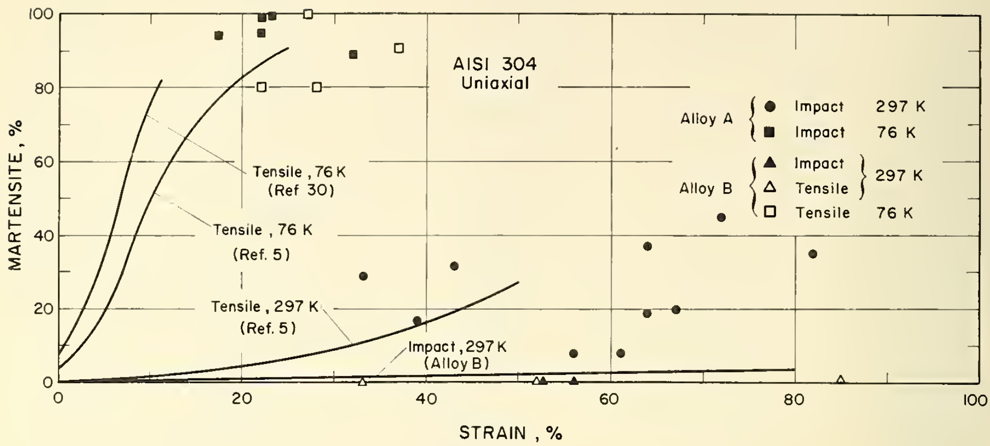

Figure 41. Formation of martensite during tensile and impact tests.

seem to be much more dependent on alloy composition than they are at 76K.

In all of the 304 samples, the martensite fraction was recorded after fracture. The results in Figure 42 indicate that this value falls within rather narrow limits for each temperature and geometry.

5.4 Microscopic Observations

Tensile specimens of 304 and 310 stainless steels, both impact and slowly loaded (0.002 min^{-1}), were examined using techniques of optical and transmission electron microscopy. Specimens were deformed in tension at either 76 or 297K to produce strains of approximately 3% or 9%. After a specimen was strained, it was examined using optical light microscopy to determine the nature of the slip traces resulting from the deformation. Following this, the specimen was subsequently chemically thinned and then electropolished to produce

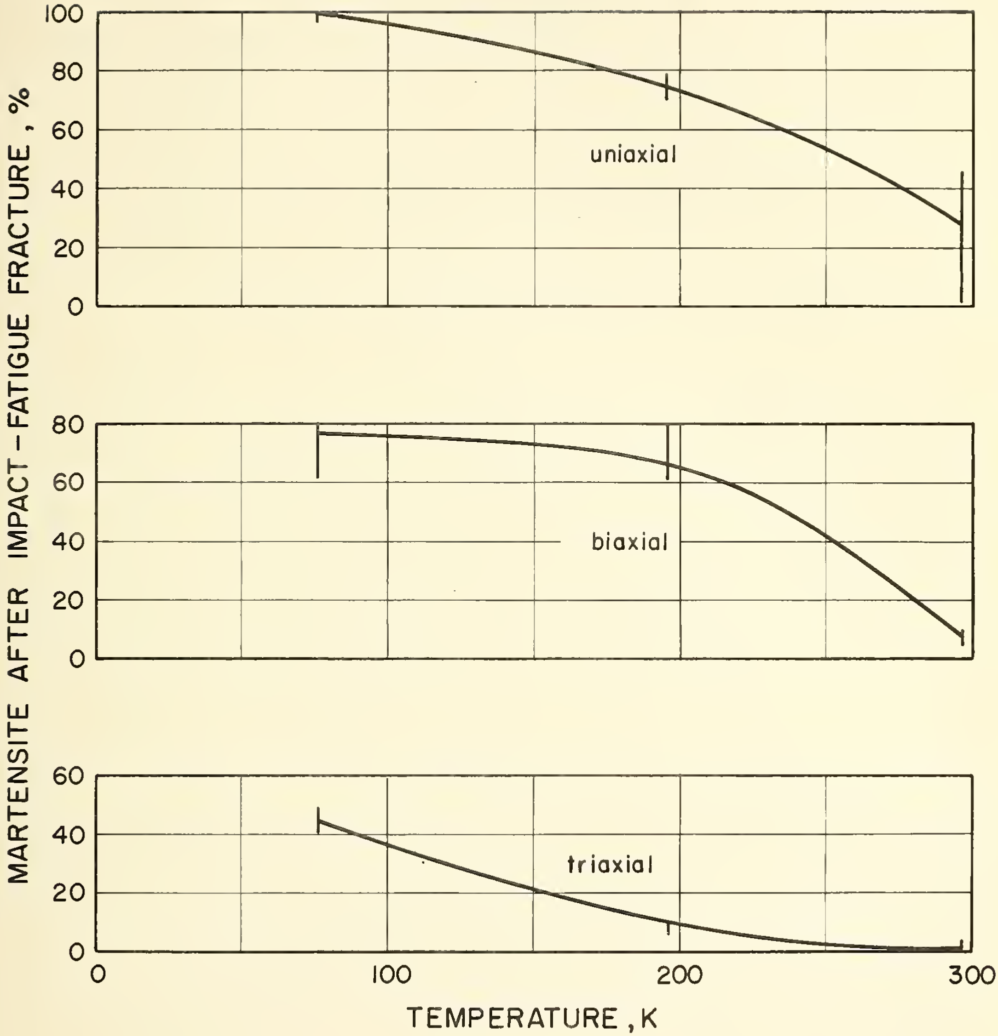

Figure 42. Temperature dependence of martensite formed after impact-fatigue fracture in AISI 304.

foils suitable for examination in the electron microscope.

Examination of the tensile specimens, using optical microscopy, revealed the grain size and slip traces. When a grain is deformed, slip will occur initially on the slip system where the resolved shear stress exceeds the critical resolved shear stress, τ_c. In face-centered cubic metals and alloys, there are 12 possible slip systems, defined by the four $\{111\}$ slip planes which each contain three $\langle 110 \rangle$ slip directions. In polycrystalline specimens, the primary slip system (the slip system on which τ_c is first exceeded) is dependent on the orientation of a grain in respect to the applied load; therefore, for grains of different orientations, slip will produce slip traces in different directions relative to one another, delineating individual grains. Furthermore, initiation of conjugate slip, slip on a second slip system, is dependent on the orientation of a grain. Figure 43 shows an area of a specimen that was strained $\sim$ 3% where there are examples of grains having slip on the primary slip system only (grain A) and grains showing cross slip (grain B), slip on both the primary and conjugate slip systems (this is representative of both 304 and 310). The frequency of grains containing cross slip is an indication of the amount of plastic deformation in a specimen, since a random distribution of orientations for the grains in each specimen can be assumed. For both alloys, it was observed that there were substantially more cross slipped grains at 9% strain than at 3% strain and that the rate of loading did not affect the occurence of cross slip. The temperature of deformation likewise did not affect the frequency of observed cross slip. This is unexpected since τ_c is temperature dependent. It, therefore, appears that the application of the tensile load, either impact or slow, and the temperature of deformation had little influence on the slip behavior of these alloys.

Face-centered cubic alloys undergo three distinct stages of deformation characterized by three dislocation structures. These are as follows:

Stage I: low strain

(a) Long straight dislocations on the primary slip system.

(b) A few dislocation interactions, the beginning of conjugate slip.

(c) More dislocation interactions.

(d) Dislocation density at end of Stage I $\sim 10^9$ cm^{-2}.

Stage II: intermediate strain

(a) Rapid appearance of rough dislocation cell structure; not possible to distinguish individual slip planes.

(b) High density of loops in cell walls.

(c) Dislocation density at end of Stage II $\sim 10^{11}$ cm^{-2}.

Stage III: high strain to rupture

(a) Misorientation between cells increases.

(b) Boundaries of cells show a tendency to lie along primary or conjugate slip traces.

Evidence of Stage I is observed for both 304 and 310 stainless steel independent of deformation temperature (the deformation of 304 is complicated by a stress-induced martensitic reaction which will be discussed later). Figure 44 shows an example of deformation characteristics of the later part of Stage I for 310 stainless steel, which corresponds to ~ 3% strain. The figure shows, as indicated by the arrows, the existence of two active slip systems, as well as dislocations which have interacted after piling up at (a) where two slip planes intersect; at (b) there is a stacking fault separating two partial dislocations. For ~ 9% strain in the same alloy, which corresponds to early Stage II, a typical dislocation structure is given in Figure 45, which shows the initiation

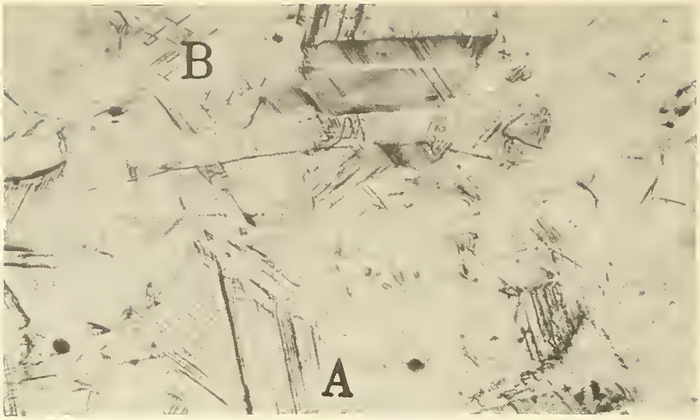

Figure 43. 304 specimen strained ~ 3%; "A" grain with slip on primary slip system only, "B" grain showing slip on two systems. 200X

Figure 44. 310 stainless steel strained ~3%. Arrows indicate slip systems; (a) are dislocation interactions at dislocation pile-up where two slip planes intersect and (b) is a stacking fault separating two partial dislocations. 40,000X

of a cell structure and a substantially higher dislocation density. The dislocation structures of 310 seemed to be the same, independent of loading and temperature; whereas the 304, while having the same general dislocation arrangements as the 310 at a corresponding strain, contained deformation twins in some grains when impacted to ~9% strain (Figure 46).

Furthermore, since 304 stainless steel undergoes a stress induced martensitic transformation, the 304 specimens both impacted and slowly strained ~9% at 297K, and all specimens strained at 76K contained hexagonal close-packed, ϵ, and body-centered cubic, α', phases associated with the transformation. Figure 47 shows an electron micrograph (a) and its selected area diffraction pattern (b) for a 304 stainless steel which has transformed after deformation. The diffraction pattern contains spots corresponding to the γ, the parent face-centered cubic phase, ϵ, and α'. The long parallel bands in the micrograph are ϵ and the dark lenticular rods in the ϵ are the cross-sections of α' lathes. In this micrograph it is evident that α' has transformed on two different variants, (a) and (b), of its habit plane. At low strain and 76K, there is evidence that ϵ is not always associated with the α', as can be seen in Figure 48. When subjected to high strains at room temperature or even low strains at 76K, independent of the method of loading, 304 stainless steel undergoes a martensitic transformation producing α' and ϵ, which is associated with dislocation structures similar to those of 310 under similar conditions of deformation.

Optical microscopy observations of fractured specimens revealed that, in general, the fracture path is random, following neither grain boundaries nor planar (martensitic) features within the grains. Other microcracks were not detected. Since all specimens exhibited

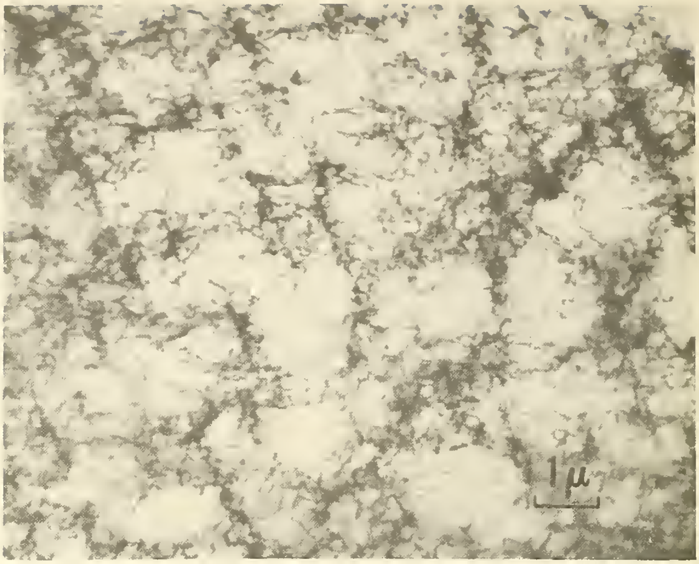

Figure 45. Cell dislocation structure of 310 stainless steel after strain of ~9%. 40, 000X

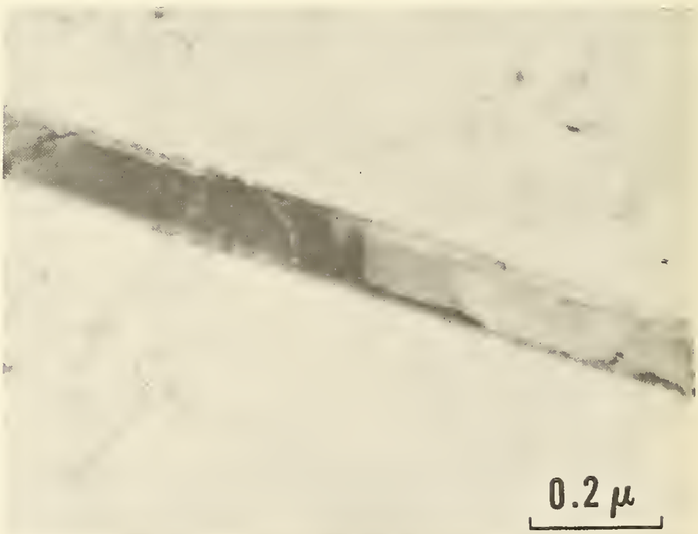

Figure 46. Deformation twin in 304 stainless steel after ~9% strain. 100, 000X

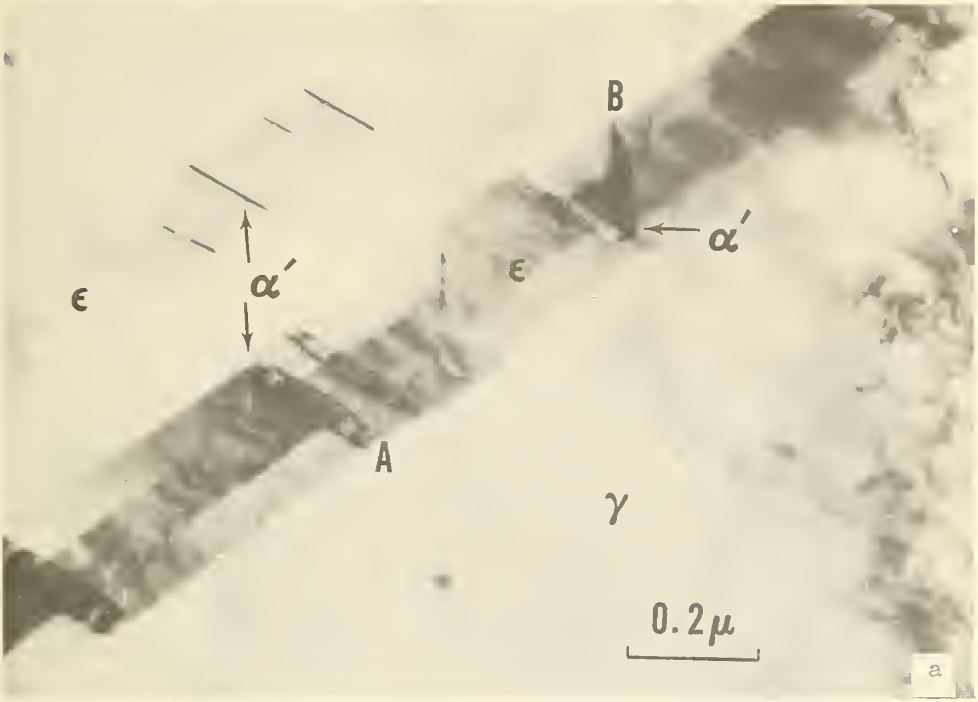

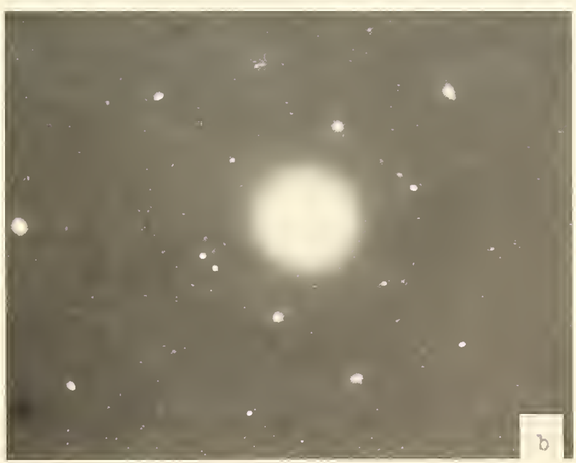

Figure 47. 304 stainless steel strained ~9%. (a) Electron micrograph at 100,000X; (b) selected area diffraction, ε (hcp), α′(bcc), and γ(fcc).

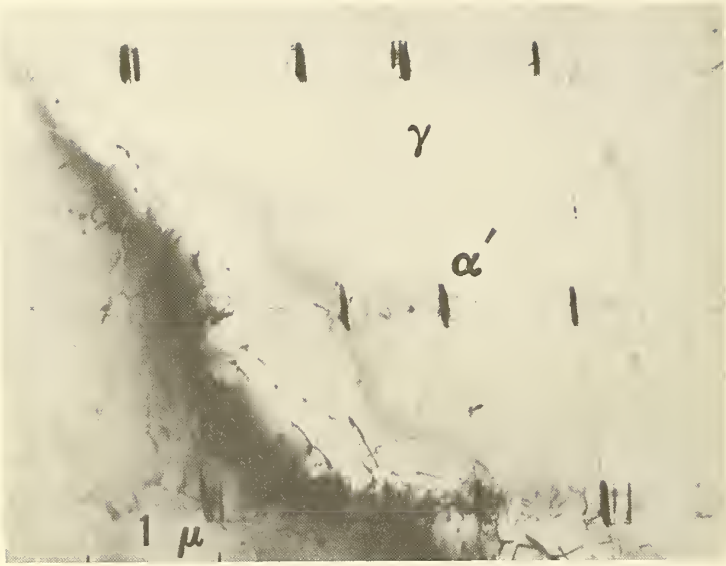

Figure 48. 304 stainless steel strained ~3% at 76 K; α' and γ present but no ϵ. 16,000X

some necking prior to fracture, it is not surprising that other cracks were not observed; the necking served to concentrate the stress within a very limited region of the specimen.

Table 5 summarizes the deformation structures and the phases present for the alloys investigated under different conditions of testing.

Table 5.

Summary of Deformation Structure and Phases Present for Deformed Alloys

Alloy	Testing Temp.	Loading	~ % Strain	ε (hcp)	α' (bcc)	Deformation Twins	~ Dislocation Density (cm^{-2})
304	297	impact	9	present	present	present	10^{11}
304	297	slow	9	present	present	none	10^{11}
304	76	slow	9	present	present	none	10^{11}
304	76	slow	3	present	present	none	10^{9}
310	297	impact	9	none	none	none	10^{11}
310	297	slow	9	none	none	none	10^{11}
310	297	impact	3	none	none	none	10^{9}
310	297	slow	3	none	none	none	10^{9}

6. Discussion

6.1 Impact-Fatigue Equipment

A new apparatus, designed to simulate the application of repeated variable loads at high strain rates on controlled specimens, has been employed in this study. The test results, using this "impact-fatigue" machine, have proven very consistent. Applied stress versus number of cycles to failure (S-N) curves blend very well with conventional "push-pull" or flexure fatigue curves (Figure 15). Since only ductile specimens (AISI 310, 304) were tested, it is of considerable interest to employ this equipment in the study of the characteristics of higher strength aerospace alloys. Presumably, crack propagation behavior under impact loading would vary considerably from high cycle fatigue loading conditions.

6.2 Fatigue Strength

Apparently, no previous fatigue studies of austenitic stainless steels have included AISI 310; this investigation represents the first documentation of AISI 310 in the temperature range 76 to 297K. As Figures 4-6 suggest, the fatigue strength increases with decreasing test temperature and is stronger for uniaxially-applied impact loads. While the ratio of the yield strength at 76K to the yield strength at 297K is about 2.6, the ratio of the increase of fatigue strength between the two temperatures is considerably less, only about 1.6. This ratio decreases more if the impact stresses are applied biaxially or triaxially.

Triaxial AISI 310 endurance limits are less than the corresponding yield strengths at each temperature. In fact, all triaxial S-N curves appear to merge at longer fatigue lives and to have endurance strengths of about 20,000 psi at over 10^4 cycles. This strength represents the lowest design stress level found for AISI 310 and is independent of operating temperature in the interval 76 to 297K.

Fatigue strengths of AISI 304, (Figure 7-9) exhibit the same trends as AISI 310. In general, however, at given fatigue life, temperature, and stress conditions, the fatigue strength of AISI 304 is slightly higher. Also, AISI 304 endurance limits are better, with the minimum endurance strength of about 25 to 30,000 psi under triaxial loading conditions at all temperatures. Again, under triaxial conditions at longer fatigue life, the effect of temperature is insignificant.

Compared to tensile yield strengths, the fatigue strength in uniaxial and biaxial conditions increases more as the test temperature is lowered (yield strength ratio, 76 to 297K, of about 1.3; fatigue strength ratio, 76 to 297K, of about 1.7). This is opposite to the effect of temperature on AISI 310 yield strength and fatigue strength ratios. But, the ratio of fatigue strength increase with decreasing temperature for the two alloys is nearly identical (AISI 310 $\simeq$ 1.6, AISI 304 $\simeq$ 1.7). This implies that the effect of martensite formation on fatigue life is relatively insignificant; in AISI 304 significantly more martensite forms in the 76K specimens than forms in the 297K. This conclusion is startling since purer martensitic alloys (Fe-Ni alloys, AISI 400 series) are well known to exhibit more brittle behavior at lower temperatures.

Even under triaxial loading conditions, when the effect of temperature becomes insignificant, (implying some embrittlement at lower temperatures) the argument cannot be made that martensitic transformation is responsible; the same trend is found in AISI 310, where no martensite was observed (see Table V). As AISI 310 yield strengths are equivalent or better than AISI 304 tensile yield strengths, the slightly better fatigue strengths obtained in AISI 304 may be attributed to martensite formation. The same explanation is usually presented for the higher ultimate strengths obtained in AISI 304, compared to AISI 310 at 76K (see Table IV). Therefore, after examination of AISI 310 (which has no stress-induced transformation) and AISI 304 (which has a stress-induced transformation) impact-fatigue data, no deleterious behavior can be attributed to the martensitic transformation. Reduction of endurance strengths under triaxial loading conditions is almost identical in both alloys, indicating that face-centered cubic alloy dislocation interactions or deformation twins are responsible, not martensitic transformations.

6.3 Welding Effects

In the course of this program, other variables such as weld properties, the effects of cold work, and the effects of thermal cycling between 76 and 297K (to produce about 5% martensite in AISI 304) were examined. Some of the results are briefly discussed below.

If AISI 304 is carefully welded, using the heliarc process, impact-fatigue strengths of the weld area are approximately 15% lower than the parent material strengths (see Figures 10 and 11). Weld tensile strengths (Table IV) are also lower than parent material strengths, as fractures occurred in the weld portion of specimens. Fatigue strengths at 10^4 cycles to failure are compared in Figure 14 for AISI 304 (welded), AISI 304 (annealed) and AISI 310 (annealed). Under biaxial loading conditions, the welded AISI 304 is about 15% weaker than the annealed materials. Unfortunately, it was not possible to manufacture triaxial specimens (round, notched) from the 1/8 inch thick sheet specimens. But the data of Figure 14 do imply that the weakest portion of a welded, AISI 304 structure would be that section which is welded and exposed to triaxially oriented loads under impact conditions. At 10^4 cycles, the impact-fatigue strength of such sections would be about 20,000 psi or greater. The endurance limit of welded, triaxially loaded specimens, however, would likely be less, 10,000 psi being a reasonable, though conservative estimate. One can arrive at this minimum stress estimate by extrapolating the welded uniaxial and biaxial fatigue strengths to triaxial strengths, using the trend of the annealed AISI 304 fatigue strengths as a guideline.

6.4 Thermal Cycling Effects

It was thought that thermal cycling to induce martensite formation spontaneously would, perhaps, alter the impact-fatigue behavior. Earlier, we had shown that prior transformation in polycrystalline AISI 304 reduces the "easy glide" portion of the stress-strain curve at 76K.[5] This "easy glide" region was shown to correspond to formation of hexagonal close packed martensite during plastic straining. Perusal of Figures 7 and 8 indicate that previous formation of small amounts of martensite has no detectable effect on subsequent impact-fatigue life.

6.5 Cold Working Effects

Cold working of AISI 310 or 304 at 76K significantly increases the subsequent impact-fatigue properties at 76 and 297K (see Figure 17). It is interesting to compare the ratios of the fatigue strengths (at 10^3 cycles) of the cold worked to annealed conditions. Both AISI 304 and 310 at 76 and 297K have ratios (fatigue strength, cold worked/fatigue strength, annealed) of between 1.4 and 1.5. This again strongly implies that martensite formation has little effect on fatigue behavior, since cold working of AISI 310 produced no martensite, while cold working of AISI 304 produces about 12% hexagonal close packed martensite and 50% body-centered cubic martensite (see Reed, Guntner[30] for martensitic product dependence on applied stress or plastic strain).

The data contained in Figures 15 and 16 indicate the high degree of correlation between our results and the conventional fatigue test results of others.[15-22] It proves informative to compare Figure 15 with the tensile results of Figure 40. At one cycle, equivalent to a high strain rate tensile test, the "fatigue" strength corresponds very well to the tensile strength. At lower applied stresses (higher cycles to failure) the endurance strength falls to approximately the minimum yield strength (20,000 psi).

6.6 Fatigue Fracture Stress

If the data is converted to fatigue fracture stress (applied load/ reduced area at fracture), the temperature dependence of the data is considerably less. In particular the biaxial and triaxial results for both AISI 304 and 310 are essentially independent of temperature. Slight temperature dependence is shown by the uniaxial data.

6.7 Deformation Energy Density

Consideration of the energy density curves in Figures 26-33 leads to some interesting speculation. It is clear that as the impact load is decreased, providing longer fatigue life, the energy absorbed by the specimen prior to fracture is reduced toward zero. For this to occur, localized deformation must replace more uniform, "tensile-type" deformation. That is, it is very likely that crack initiation processes are changing as a function of applied load. Although for simplicity the energy density-cycles to failure curves are characterized as a linear function in Figures 26-33, it is very probable that the function becomes asymptotic to zero load as the number of cycles to failure continue to increase. Following this, it is reasonable to speculate that zero energy density represents the material endurance limit; impact loading, below the stress necessary to produce some finite specimen strain, will never produce specimen fracture. Of further interest is the tendency of all assumed linear functions (energy density versus cycles to failure), if extrapolated, to converge to zero energy density at the same number of cycles to failure (see Figures 27, 28 and 31, for example).

6.8 Martensite Formation in AISI 304

Martensite formation was monitored as a function of number of cycles, and the results are presented in Figure 36. The increase of martensite (a ferromagnetic phase) with increasing number of fatigue cycles promotes the feasibility of monitoring fatigue life. The undeformed material, austenite, is paramagnetic; therefore, magnetometric monitoring of specimens or components exposed to repeated loads should very easily indicate impending fracture.

The monitored specimen, tested at room temperature, exhibits an unusual increase in uniform reduction in area, elongation, and percent martensite transformed just prior to fracture (Figure 36). To our knowledge, the rather sudden increase in uniform specimen strain (not specimen necking) has not been reported in the literature and is quite unexpected. Further consideration and documentation of this is needed. Arguments cannot be advanced that fracture propagation is solely responsible, since little uniform martensite transformation would be expected to occur except along fracture paths.

6.9 Tensile Data

Compiled tensile data for both alloys, shown in Figure 39 and 40, indicate the increase of AISI 310 yield strength, compared to AISI 304, at lower temperatures. Again, the lower 304 yield strength can be attributed to hexagonal martensite formation. Higher 304 tensile strengths have been attributed to body-centered martensite strengthening. Further discussions of these contributions are contained in many references.[5,29,30]

Figure 41 contains data on martensite (b.c.c.) formation as a function of specimen strain for comparison of impact-loaded and tensile-loaded specimens. Room temperature data of Alloys A and B do show significant difference. Both of these alloys are commercially classified and sold as AISI 304, but it is easy to discern their different transformation characteristics. This difference is also apparent at 76K. Comparison of the effect of strain rate on transformation tendency is not as conclusive. From our available data,no definitive statement can be made related to this question, although many others claim that increased strain rate produces lower amounts of martensite per unit strain.[3,9,24,25]

6.10 Microscopy

Discussion of optical and electron microscopy results is presented in the Experimental Results section. Several observations provide points for additional discussion. All specimens examined had necked prior to crack propagation and fracture. In this sense, therefore, fracture was very similiar to conventional tensile fracture, as contrasted to fatigue crack propagation and fracture. Martensite played no detectable role in crack propagation, nor were premature cracks initiated by the martensitic structures.

It is well documented that high energy rate forming of face-centered cubic metals produces an abundance of deformation at ambient temperatures or higher. Similarly, impact-loading of AISI 304 produced deformation twins (see Table V), however, none were found in 310. As suggested by many (see Venables[31] for review), this evidence supports the view that lower stacking fault energy promotes twinning. At lower temperatures in 304, martensitic transformations (hcp and bcc) evidently replace twinning as deformation products.

6.11 Possible Additional Programs

There are indications [32] that the fatigue strengths of AISI 300 Series steels which undergo partial martensitic transformations are less at 20K in the large amplitude range than at 76K. Therefore, it should be clearly understood that the conclusions drawn in the report only apply in the temperatures range 76 to 294K. Additional data should be acquired below 76K to enable accurate prediction of the long-time life of components exposed to periodic sudden loads in this temperature regime.

7. References

1. P. P. Benham, Metallurgical Reviews 3, 203 (1958).
2. J. D. Campbell and J. Duby, Proc. Roy. Soc. (London) A236, 24 (1956).
3. H. G. Baron, J. Iron Steel Inst. 182, 354 (1956).
4. J. D. Campbell, J. Duby and K. E. Puttick, Phil. Mag. 2, 548 (1957).
5. C. J. Guntner and R. P. Reed, Trans. ASM 55, 399 (1962).
6. T. Williams, Sheet Metal Industries 39, 487 (1962).
7. S. W. Hollingum, High Energy Rate Working of Metals, Proc. NATO Advanced Study Institute, Central Institute for Industrial Research, Oslo, Norway, 278 (1964).
8. T. Kvam and B. Augland, source cited in ref. 7, p. 264.
9. J. P. Bressanelli and A. Moskowitz, Trans. ASM 59, 223 (1966).
10. L. E. Murr and T. I. Grace, Expt. Mech. 9, 145 (1969).
11. D. V. Neff, T. E. Mitchell, and A. R. Troiano, Trans. ASM 62, 858 (1969).
12. A. Kumar and R. G. Kumble, J. Appl. Phys. 40, 3475 (1969).
13. A. Kumar, High Speed Testing Vol. VII: The Rheology of Solids, Interscience Publishers, N. Y., 67 (1969).
14. R. N. Orava and H. E. Otto, J. Metals 22 #2, 17 (1970).
15. R. M. Brick and A. Phillips, Trans. ASM 29, 435 (1945).
16. D. W. McDowell, "Low Temperature Properties of Type 304 Stainless Steels", Technical Report, Development and Research Division, The International Nickel Co., New York (1959).
17. E. Krempl, "Notch High-Strain Fatigue Behavior of Three Low-Strength Structural Steels, General Electric Co., Atomic Power Equipment Dept., San Jose, Calif. (1969), NTIS GEAP-5714.

18. K. Fushimi, H. Okamato, E. Fukishima, and H. Yonemitsu, Low Temperature Engineering 5, 105 (1970).

19. J. T. Berling and J. B. Conway, Met. Trans. 1, 805 (1970).

20. M. G. Fontana, "Investigation of Mechanical Properties and Physical Metallurgy of Aircraft Alloys at Very Low Temperatures, Pt. II", Tech. Rept. 5662, Ohio State Univ. Research Foundation (1948).

21. J. L. Zambrow and M. G. Fontana, Trans. ASM 41, 480 (1949).

22. J. W. Spretnak, M. G. Fontana, and H. F. Brooks, Trans. ASM 43, 547 (1951).

23. A. Kramer and W. M. Baldwin, Jr., Trans. ASM 50, 803 (1958).

24. B. Eftestøl, B. F. Haegland, P. Storvik, and A. Windfeldt, source cited in ref. 7, p. 296.

25. G. W. Powell, E. R. Marshall, and W. A. Backofen, Trans. ASM 50, 478 (1958).

26. J. F. Watson and J. L. Christian, Report ERR-AN-057 of Third Quarterly Progress Report - Phase I, Contract AF 33(616)-7984, Dec., 1961, General Dynamics/Astronautics, San Diego, California, NTIS AD 273221.

27. C. J. Guntner and R. P. Reed, Advances in Cryogenic Engineering, Vol. 6, K. D. Timmerhaus, Ed., Plenum Press, Inc., New York (1961), p. 565.

28. K. A. Warren and R. P. Reed, "Tensile and Impact Properties of Selected Materials from 20 to 300°K", National Bureau of Standards Monograph 63 (1963).

29. A. J. Nachtigall, "Comparison of Tensile Properties of 304 L and 310 S Stainless in Liquid Helium", NTIS NASA-TM-X-52703 (1969).

30. R. P. Reed and C. J. Guntner, Trans. Met. Soc. AIME 230, 1713 (1964).

31. J. A. Venables, Deformation Twinning, Met. Soc. Conf. Vol 25, (Gordon and Breach Science Publ., N. Y. 1964) p. 77.

32. F. Schwartzberg, "Cryogenic Materials Data Handbook", ML-TDR-64-280 (PB171809), Clearinghouse for Tech. and Sci. Inform., Washington D. C. (1968).

Appendix

The following paper, "Apparatus for Impact-Fatigue Testing," describes the modifications made to automate a standard impact machine. It has been accepted for publication in Section C, Journal of Research, NBS (1971).

Another paper summarizing the main findings in this report is presently in progress.

Apparatus for Impact-Fatigue Testing*

R. E. Schramm, R. L. Durcholz and R. P. Reed
Cryogenics Division, NBS-Institute for
Basic Standards, Boulder, Colorado, 80302

A standard impact machine was extensively modified to allow the measurement of the response of specimens to repeated, controlled impact pulses. This equipment enables one to vary the temperature (76 - 297K), specimen geometry (uniaxial, biaxial, triaxial stress systems), and load levels. At stress levels in the neighborhood of the yield stress on the order of 10,000 impact cycles are needed to fatigue specimens to fracture. Strain rates achieved are moderately high, of the order of 1000 min^{-1}, which conveniently form intermediate data between tensile (max. of about 100 min^{-1}) and explosive straining data (about 6000 min^{-1}). Contrasted to standard fatigue tests, no constraint is placed on specimen elongation and only unidirectional stresses are imposed. Typical impact-fatigue results for AISI 310 stainless steel are presented.

Key words: Cryostat; fatigue; impact; low temperature; mechanical property equipment; stainless steel.

---

* This work was carried out at the National Bureau of Standards for the Naval Air Engineering Center, Philadelphia, Pennsylvania.

1. INTRODUCTION

In many low temperature applications such as in the transportation of dewars or in the transfer of cryogenic liquids through pipe, system components experience periodic sudden jolts or loads. Prediction of expected life of these components can best be accomplished by testing controlled specimens under repeated impact loads which approach up to the yield load. Such a test, then, can be described as impact-fatigue, as the specimen eventually fractures in a manner similar to conventional fatigue fractures.

To perform such tests a standard commercial impact machine was extensively modified. These modifications resulted in an apparatus that could repeatedly apply sudden loads in the range 0 to 1800 kilograms for the many repetitions sometimes required for specimen fracture. Additionally, the specimen chamber was insulated to allow temperature environments from 76 to 297K. Our paper describes this new equipment.

A standard Riehle model PI-2* impact testing machine was available. This machine has three hammer sizes, 15, 30, and 60 lbs. (6.8, 13.6 and 27.3 kg) and the hammer drop is continuously adjustable from 0 to 48 inches (0 to 1.3 m). Our impact-fatigue life determinations, however, would require greater than 20,000 cycles in some cases so it became obvious that the single cycle operation for which this machine was designed was not feasible. We designed major modifications to automate the repetition, to allow tests to be conducted at cryogenic temperatures, and to permit the use of specimens in a great variety of configurations. Stress pulses are applied to the specimen in one direction, while the conventional fatigue tests are typically either "push-pull" with alternating tensile and compressive forces or flexure with alternating applied bending forces. Another feature of the impact-fatigue test is that the specimen is not constrained with respect to specimen strain.

---

* The use of trade names in this paper in no way implies endorsement or approval by NBS and is included only to define the experimental procedure.

2. MODIFICATIONS

Figure 1 a is a schematic view of the impact-fatigue tester. A 1/6 hp, 1725 rpm electric motor is geared to rotate a 24 inch diameter wheel at 7.3 rpm. The shaft and bearings which support this wheel are clamped to the upright part of the impact machine frame by U-bolts. A brass hammer release arm protruding through the outer edge of this moving wheel serves to pick up the hammer and raise it to a predetermined height. At this point, the trip arm (Fig. 2) encounters a block which is supported behind the rotating wheel. The trip arm rotation causes a cam motion which swings a locking bar out of position allowing the hammer release to simply fall back under the weight of the hammer. A second trip block is at the top of the wheel's revolution to insure that the system does not bind there as it passes the pendulum shaft. After each trip, springs pull the release bar back into a locked position to repeat the cycle.

The standard anvil on the base of the impact machine has been closed off on the right end to serve as the fixed point to which the right specimen pull rod is anchored, either directly or through a load cell (Fig. 3). The left pull rod passes through a three piece impact yoke assembly held together by eight $\frac{1}{4}$ inch stainless steel bolts. The hammer impact is absorbed by this yoke which transmits it to the specimen, since it is free to move in a right-left direction on four rollers. When the sample breaks, the yoke moves to the left and allows the hammer to strike a switch on the base which removes electrical power from the whole system.

A solenoid system prevents secondary impact by the recoiling hammer (Fig. 1). This stop is a 3/4 inch round bar which rides in a brass bushing inserted into a drilled hole in the impact machine. When this bar is in the fully inserted position, the impact hammer cannot swing past it to strike the yoke. A portion of the bar has a flat depression ground into it so that when the solenoid is activated and the bar partially withdrawn from the anvil the hammer may pass by freely. A switch on the stationary wheel near the block that trips the hammer release mechanism controls the power to the solenoid. As the

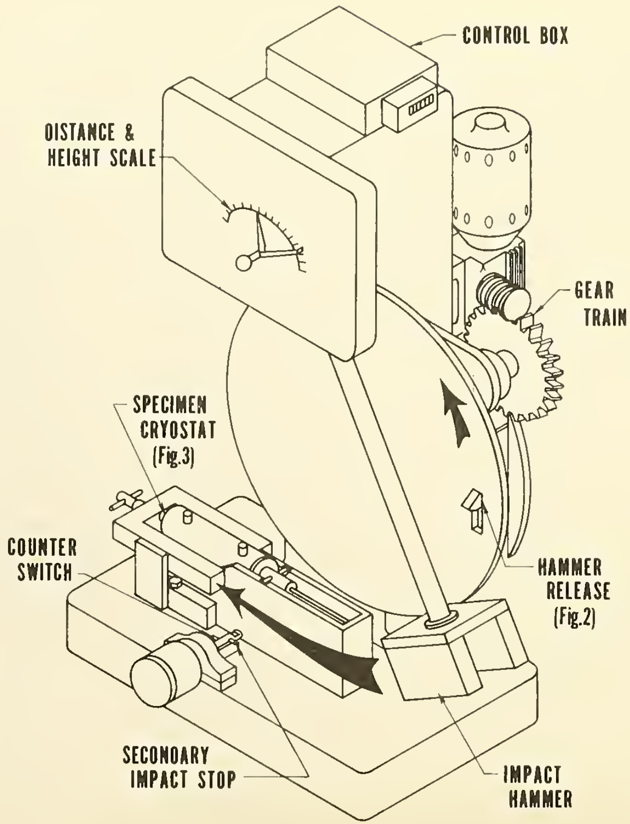

Figure 1a. Schematic view of impact-fatigue tester.

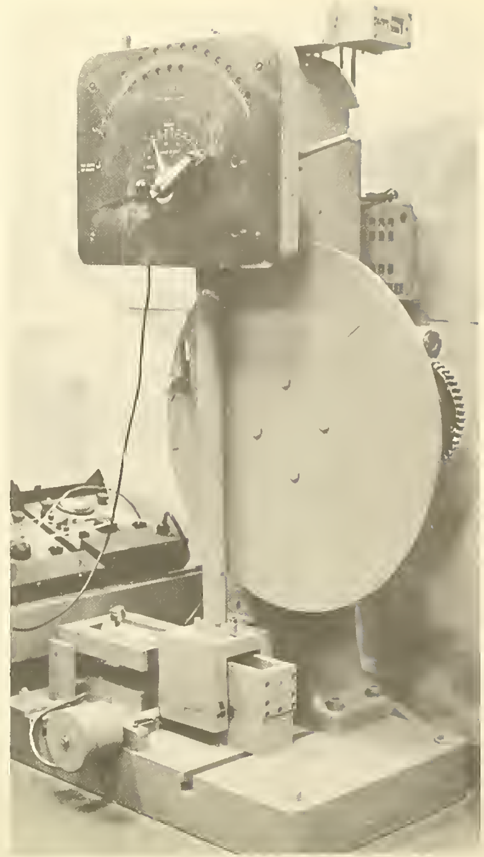

Figure 1b. Photograph of impact-fatigue tester.

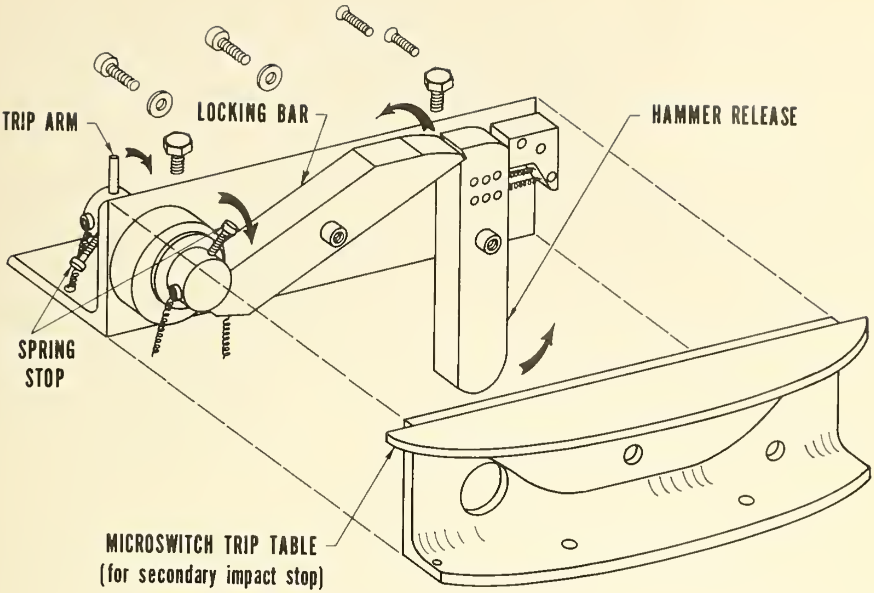

Figure 2. Impact hammer release mechanism. The trip arm is rotated by a stationary block fixed at the desired position behind the 24 inch wheel. This allows the hammer release to fall back under the hammer weight. Springs then return the mechanism to a locked position.

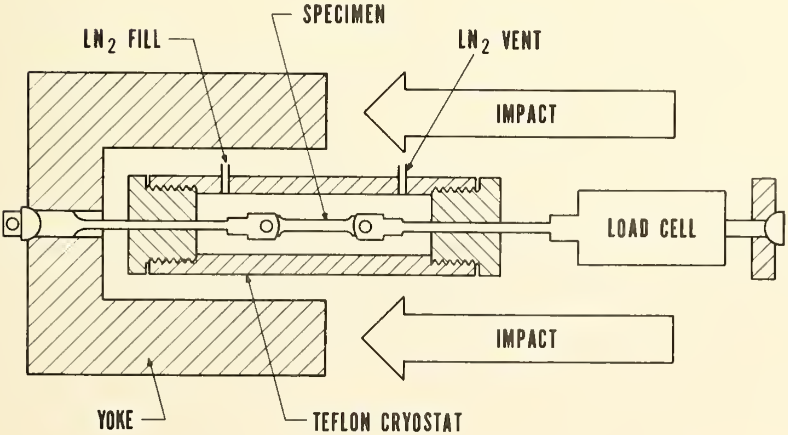

Figure 3. Specimen impact system.

trip table (Fig. 2) passes by this switch, the secondary stop is removed from the impact hammer path. By the time the hammer has recoiled, power has been removed from the solenoid and springs have pushed the stop back into position. A pin through this bar operates another switch to advance a cycle counter.

Wherever possible, the springs in the hammer-release mechanism were doubled, so if one fails during a test the second will continue to function until repairs can be made. It is important to use high quality steel springs to minimize difficulty due to breaks; soft, tempered springs were found more reliable than high strength units. Since this modification results in a much higher repetition rate than was originally intended, the welds between the pendulum shaft and fittings on both ends were reinforced.

3. CRYOSTAT

The cryostat used for 76 K tests consisted simply of a 2 inch diameter Teflon rod, 7 inches long, with a 1 inch bore through the center. The specimen pull rods are supported and centered by Teflon end caps screwed into the main chamber (Fig. 3). Rubber O-rings in both of these caps served as an initial seal around the pull rods to minimize the loss of liquid nitrogen. However, in cooling to 76 K, the Teflon contracts considerably and then serves as the main seal. Because of this great contraction, it is necessary to check for free movement of the pull rods when they are at test temperatures. Two small holes in the side wall serve for filling with liquid nitrogen and venting. A liquid flow of about 6 ℓ/hr was generally used to maintain temperature. At room temperature this cryostat was still used to assure the proper positioning of the sample.

For 195 K tests, a slight modification of this system was employed. Instead of the small holes in the side wall for filling and venting nitrogen, a 1×4 inch panel was removed. A styrofoam box was attached to act as a reservoir for the powdered dry ice used to fill the cryostat. Consumption in this case was about 0.5 lb/hr.

4. DISCUSSION

We used a load cell specially constructed to withstand sudden impacts and a high speed recorder to measure impact loading. When using the 30lb. (13.6kg) hammer, the impulse time is about 2 msec. Load cell response (Fig. 4) indicates a damped ringing, but this is a characteristic of the load cell. While the specimen probably does vibrate in the uniaxial direction, our system is incapable of measuring the compressive forces it may experience, but they are believed to be very small.

During the progress of a test the specimen undergoes plastic strain. This allows the yoke to move in the direction of motion of the impact hammer. Thus, by measuring the position of the yoke frequently during a test, it is possible to determine specimen strain as a function of the number of cycles. Naturally, this function depends on variables such as material, temperature, and applied pulse. Figure 5 illustrates a typical curve of strain versus number of cycles for an AISI 310 stainless steel specimen. Initially, the specimen undergoes considerable strain but, after sufficient work hardening (several hundred cycles), its length becomes nearly constant.

Since each cycle corresponds to a 2 ms impulse time, the coordinate giving the number of cycles is also a time coordinate and its slope gives the strain rate. With our experimental conditions, the maximum initial strain rate was 2100 min^{-1}. This is conveniently intermediate between the maximum strain rate in tensile tests of about 100 min^{-1} and the approximate lower limit[1] in explosive straining of 6000 min^{-1}.

From the strain readings and load calibration, a typical stress-strain curve may be constructed. Figure 6 shows this curve for AISI 310 at 297 K. The stress used to construct this curve is the engineering stress, i.e., load divided by original area. This stress level is constant throughout the test.

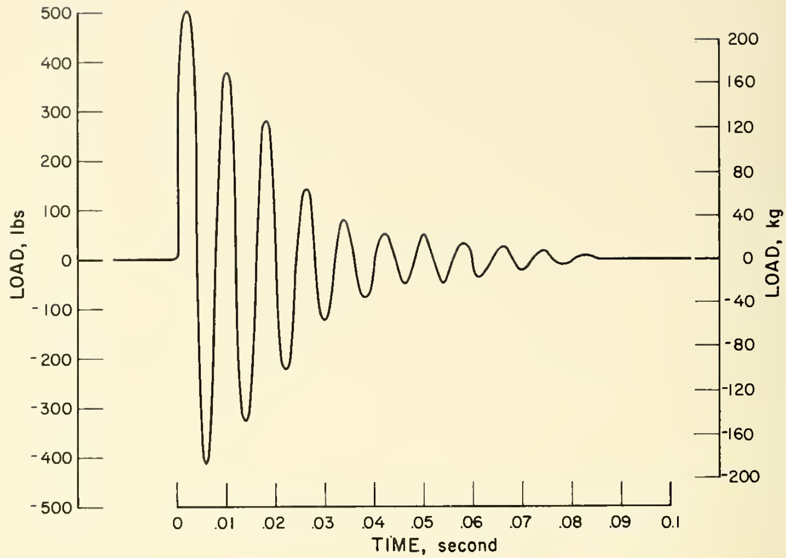

Figure 4. Time response curve recorded by load cell and high speed recorder.

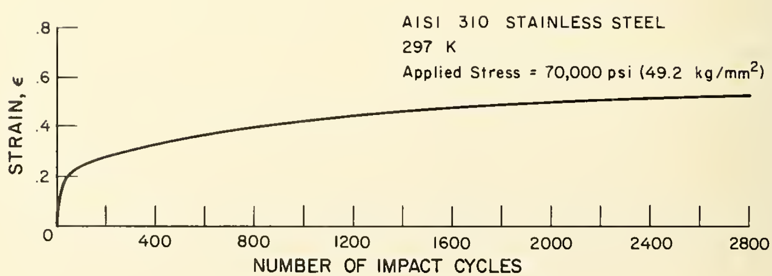

Figure 5. Specimen strain during impact-fatigue life.

By varying the height of the hammer (stress amplitude), a typical fatigue (S-N) curve of stress level versus number of cycles to failure may be obtained. The shape of such curves for AISI 310 at 297, 195 and 76 K, as shown in Fig. 7, is very similar to those obtained by conventional fatigue tests in which the high strain rates are not achieved and either the load or specimen deflection amplitude is held constant.

Any specimen configuration, limited only by length (about 5 inches), may be measured. In practice, we have measured both uniaxial (tensile), biaxial, and triaxial (notch tensile) specimens of both AISI 304 and 310 stainless steels at 76, 195 and 297 K. These test results will be published later.

5. REFERENCES

[1] E. K. Henriksen, I. Lieberman, J. F. Wilkin, and W. B. McPherson, "Metallurgical Effects of Explosive Straining", in Symposium on Dynamic Behavior of Materials (ASTM Spec. Tech. Pub. No. 336, 1963), p 104.

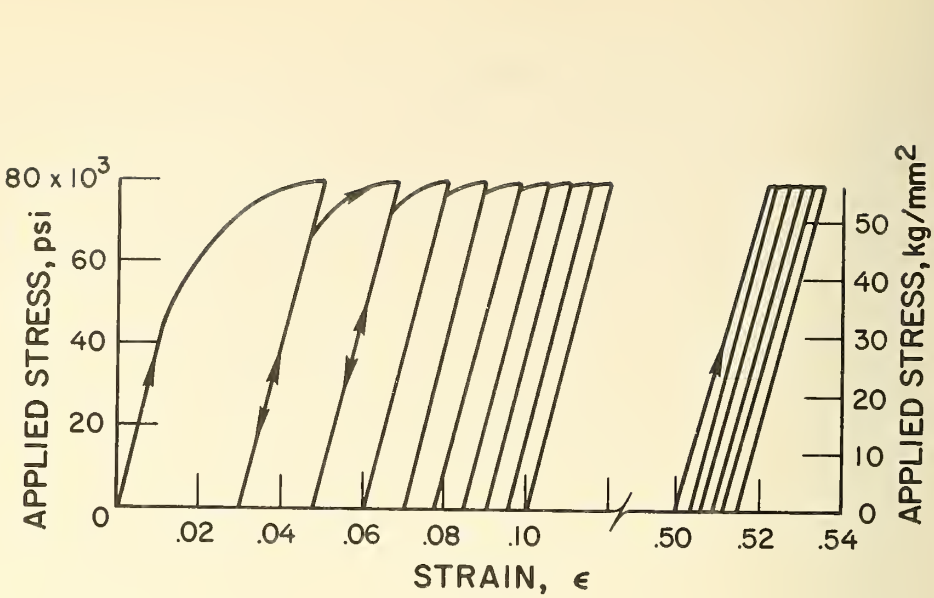

Figure 6. Typical stress-strain curve for AISI 310 stainless steel showing repeated impact cycles at 297 K (1 kg/mm^2 = 9.8 x 10^6 N/m^2). Compressive stresses due to recoil of specimen upon itself are very small and not shown.

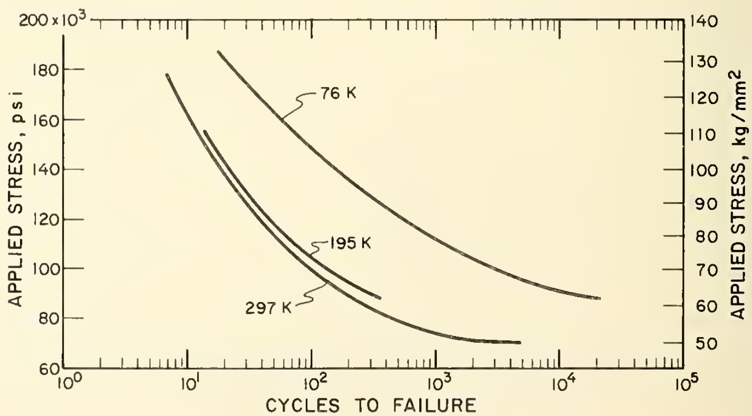

Figure 7. Fatigue life curve for AISI 310 at 297, 195, and 76 K.

FORM NBS-114A (1-71)

U.S. DEPT. OF COMM. BIBLIOGRAPHIC DATA SHEET	1. PUBLICATION OR REPORT NO. NBS-TN-609	2. Gov't Accession No.	3. Recipient's Accession No.

4. TITLE AND SUBTITLE

Study of Cryogenic Storage Tank Fatigue Life (Low Temperature Mechanical Testing of AISI 304 and 310 Stainless Steels)

5. Publication Date August 1971

6. Performing Organization Code

7. AUTHOR(S) R. P. Reed, R. L. Durcholz, R. E. Schramm, and T. J. Patrician

8. Performing Organization

9. PERFORMING ORGANIZATION NAME AND ADDRESS

NATIONAL BUREAU OF STANDARDS
DEPARTMENT OF COMMERCE
WASHINGTON, D.C. 20234

10. Project/Task/Work Unit No. 2750533

11. Contract/Grant No. 9-8029

12. Sponsoring Organization Name and Address

Naval Air Engineering Center
Philadelphia, Pennsylvania

13. Type of Report & Period Covered N/A

14. Sponsoring Agency Code

15. SUPPLEMENTARY NOTES

16. ABSTRACT (A 200-word or less factual summary of most significant information. If document includes a significant bibliography or literature survey, mention it here.)

Two 300 series stainless steels were tested for impact-fatigue life and tensile properties as a function of temperature, percent transformed phase (martensite), stress level, and specimen geometry. These alloys were studied to predict the fracture characteristics of parent material and weld joints in large cryogenic dewars which are subjected to periodic stresses. Normally, AISI 304 is employed in the construction of such dewars. Under fatigue loading conditions at cryogenic temperatures, the behavior of AISI 304 is complicated by the gradual transformation to a martensitic structure. The influence of this transformation on the fracture characteristics was studied. For this purpose, a new impact-fatigue test and necessary equipment were developed.

The fatigue strength of AISI 304 and 310 exhibit similar trends, but at a given fatigue life and temperature, the fatigue strength of AISI 304 is slightly superior. AISI 310 displays an endurance limit of about 20,000 psi*; the 304 limit is 25-30,000 psi. However, the lowest endurance limit (weakest) specimens appear to be the triaxially-loaded AISI 304 weld specimens which have an endurance limit near 10,000 psi. Little temperature-dependence of the impact-fatigue properties was observed.

* For ease in interpretation all stress values in the text are expressed in units of psi. Conversion to other stress units are

$$10^3 \text{ psi} = 0.703 \text{ kg/mm}^2 = 6.90 \times 10^6 \text{ N/m}^2$$

17. KEY WORDS (Alphabetical order, separated by semicolons) fatigue; fracture; impact; low temperature; mechanical property equipment; stainless steel.

18. AVAILABILITY STATEMENT	19. SECURITY CLASS (THIS REPORT)	21. NO. OF PAGES
[X] UNLIMITED.	UNCLASSIFIED	86
[ ] FOR OFFICIAL DISTRIBUTION. DO NOT RELEASE TO NTIS.	20. SECURITY CLASS (THIS PAGE) UNCLASSIFIED	22. Price 75 cents

NBS TECHNICAL PUBLICATIONS

PERIODICALS

JOURNAL OF RESEARCH reports National Bureau of Standards research and development in physics, mathematics, chemistry, and engineering. Comprehensive scientific papers give complete details of the work, including laboratory data, experimental procedures, and theoretical and mathematical analyses. Illustrated with photographs, drawings, and charts.

Published in three sections, available separately:

- **Physics and Chemistry**

Papers of interest primarily to scientists working in these fields. This section covers a broad range of physical and chemical research, with major emphasis on standards of physical measurement, fundamental constants, and properties of matter. Issued six times a year. Annual subscription: Domestic, $9.50; foreign, $11.75*.

- **Mathematical Sciences**

Studies and compilations designed mainly for the mathematician and theoretical physicist. Topics in mathematical statistics, theory of experiment design, numerical analysis, theoretical physics and chemistry, logical design and programming of computers and computer systems. Short numerical tables. Issued quarterly. Annual subscription: Domestic, $5.00; foreign, $6.25*.

- **Engineering and Instrumentation**

Reporting results of interest chiefly to the engineer and the applied scientist. This section includes many of the new developments in instrumentation resulting from the Bureau's work in physical measurement, data processing, and development of test methods. It will also cover some of the work in acoustics, applied mechanics, building research, and cryogenic engineering. Issued quarterly. Annual subscription: Domestic, $5.00; foreign, $6.25*.

TECHNICAL NEWS BULLETIN

The best single source of information concerning the Bureau's research, developmental, cooperative and publication activities, this monthly publication is designed for the industry-oriented individual whose daily work involves intimate contact with science and technology—*for engineers, chemists, physicists, research managers, product-development managers, and company executives.* Annual subscription: Domestic, $3.00; foreign, $4.00*.

NONPERIODICALS

Applied Mathematics Series. Mathematical tables, manuals, and studies.

Building Science Series. Research results, test methods, and performance criteria of building materials, components, systems, and structures.

Handbooks. Recommended codes of engineering and industrial practice (including safety codes) developed in cooperation with interested industries, professional organizations, and regulatory bodies.

Special Publications. Proceedings of NBS conferences, bibliographies, annual reports, wall charts, pamphlets, etc.

Monographs. Major contributions to the technical literature on various subjects related to the Bureau's scientific and technical activities.

National Standard Reference Data Series. NSRDS provides quantitative data on the physical and chemical properties of materials, compiled from the world's literature and critically evaluated.

Product Standards. Provide requirements for sizes, types, quality and methods for testing various industrial products. These standards are developed cooperatively with interested Government and industry groups and provide the basis for common understanding of product characteristics for both buyers and sellers. Their use is voluntary.

Technical Notes. This series consists of communications and reports (covering both other agency and NBS-sponsored work) of limited or transitory interest.

Federal Information Processing Standards Publications. This series is the official publication within the Federal Government for information on standards adopted and promulgated under the Public Law 89–306, and Bureau of the Budget Circular A–86 entitled, Standardization of Data Elements and Codes in Data Systems.

Consumer Information Series. Practical information, based on NBS research and experience, covering areas of interest to the consumer. Easily understandable language and illustrations provide useful background knowledge for shopping in today's technological marketplace.

NBS Special Publication 305, Supplement 1, Publications of the NBS, 1968-1969. When ordering, include Catalog No. C13.10:305. Price $4.50; foreign, $5.75.

* Difference in price is due to extra cost of foreign mailing.

Order NBS publications from: Superintendent of Documents
Government Printing Office
Washington, D.C. 20402

U.S. DEPARTMENT OF COMMERCE
National Bureau of Standards
Washington, D.C. 20234

OFFICIAL BUSINESS

Penalty for Private Use, $300

POSTAGE AND FEES PAID
U.S. DEPARTMENT OF COMMERCE

U.S.MAIL